

---

# Time-Resolved Fluorescence Anisotropy

---

Steven S. Vogel, Christopher Thaler,  
Paul S. Blank, and Srinagesh V. Koushik

## 10.1 INTRODUCTION

---

In this chapter, we will discuss how molecular rotation and protein–protein interactions can be measured using time-resolved fluorescence anisotropy—a variation of fluorescence lifetime imaging (FLIM) (Bastiaens and Squire 1999; Gadella, Jovin, and Clegg 1993; Lakowicz, Szmacinski, 1992; Wang, Periasamy, and Herman 1992). We wish to state that this chapter is not intended to be a review of the fluorescence polarization and anisotropy literature; rather, our goal is to complement the limited but growing list of recent studies where polarization and anisotropy microscopy has been applied to biological questions (Bader et al. 2007; Blackman et al. 1996; Blackman, Piston, and Beth 1998; Clayton et al. 2002; Clegg, Murchie, and Lilley 1994; Gautier et al. 2001; Heikal et al. 2000; Hess et al. 2003; Jameson and Mocz 2005; Piston and Rizzo 2008; Rao and Mayor 2005; Rizzo and Piston 2005; Runnels and Scarlata 1995; Sharma et al. 2004; Suhling et al. 2004; Traler et al. 2009; Varma and Mayor 1998; Volkmer et al. 2000; Yan and Marriott 2003; Yeow and Clayton 2007) by conveying an intuitive appreciation of the methods used for measuring anisotropy and the strengths and weaknesses of the approach, as well as identifying some of the current technical limitations.

Often in textbooks, complex methods such as fluorescence anisotropy and polarization are described using mathematical formulae. Although a formula can be a precise and concise means of conveying complex ideas between experts well trained in mathematics, the use of formulae can actually impede comprehension for a lay audience. Similarly, the use of technical jargon can aid communication between experts with a common appreciation of underlying concepts, but its use can hinder communication with the uninitiated. Alternatively, attempts to present complex methods in an intuitive fashion often require making simplifying assumptions, which can lead to confusion. Here, we attempt to avoid

these communication pitfalls by first presenting the fundamental photophysical concepts underlying fluorescence polarization and anisotropy. This we hope will provide some foundation for the more detailed explanations, occasionally using formulae, found in subsequent sections and serve as a starting point from which a thorough understanding of the theoretical principles governing the technique can be attained.

At its most fundamental level, *time-resolved fluorescence anisotropy monitors changes in the orientation of a fluorophore*. These measurements are typically monitored over a time course spanning picoseconds to nanoseconds using the time-correlated single-photon counting technology (TCSPC; Becker 2005) more commonly used for fluorescence lifetime imaging. Changes in fluorophore orientation can reflect the rotation of a macromolecule to which a fluorophore is attached. Rapid changes in fluorescence orientation (anisotropy) can also reveal resonance energy transfer between fluorophores in close proximity and, by inference, indicate that the macromolecules to which the fluorophores are attached are also in close proximity. The immediate challenge is to understand how the orientation of a fluorophore can be measured using an optical microscope.

## 10.2 UNDERLYING CONCEPTS

---

Two key concepts of photophysics are critical to gaining a clear understanding of fluorescence anisotropy imaging. The first concerns the nature of the electric field of light. This is important because the orientation of the electric field of the light used to excite fluorophores in an anisotropy experiment is used as a fiduciary orientation against which all changes in orientation are measured. The second concept involves absorption and emission dipoles of fluorophores and the role that they play in the absorption and emission of photons. The orientation of the absorption dipole of a fluorophore is important because it is a key factor that determines the probability that a fluorophore will absorb a photon to reach an excited state. Similarly, the orientation of the emission dipole of a fluorophore is important because it dictates the orientation of the electric field of the photons emitted by the fluorophore. The orientation of the electric field of these emitted photons will subsequently be used to deduce the orientation of the fluorophore itself relative to the electric field orientation of the excitation light. We begin with the nature of the electric field of light.

*The electric field of light:* Light is a form of electromagnetic radiation with wave-like behavior and composed of elementary particles called *photons*. As photons travel through space, they generate both electric and magnetic fields. The electric field of light oscillates, and the vector of these oscillations defines the orientation of its electric field. This orientation is always perpendicular to the direction in which the light is traveling and orthogonal to the vector orientation of its magnetic field. If the electric field orientation does not change as light travels through space, it is called *linearly polarized light*. This light is primarily used as the excitation light in fluorescence anisotropy experiments, and the invariant electric field orientation of the linearly polarized light source serves as a fiduciary orientation ( $\theta = 0^\circ$ ) against which other orientations are measured. We will show shortly that analyzing the orientation of the electric fields of light emitted from a sample yields information regarding the speed of molecular rotation.

*Absorption and emission dipoles:* Imaging fluorescence involves excitation by the absorption of a photon at one wavelength and the emission and detection of a photon at a different wavelength. With one-photon excitation, one high-energy photon is absorbed by the fluorophore, and a single lower energy (longer wavelength) photon is subsequently emitted. With multiphoton excitation, two or more than two lower energy photons are absorbed simultaneously by the fluorophore (Denk, Strickler, and Webb 1990).

The absorption of a photon by a fluorophore involves the excitation of an electron from a ground state to an excited state. In general, a *dipole* is formed by the separation of a positive and a negative charge. With fluorescence excitation, an *absorption dipole* defines the preferred orientation of the chromophore to absorb a photon. The orientation of this dipole is specific to the chemical structure of the chromophore (often oriented along the axis of alternating single and double bonds that define the extended p-orbital).

The probability that a fluorophore will be excited is a direct function of the relative orientations of the electric field of the excitation light and the absorption dipole of the chromophore. When the electric field orientation is parallel to the absorption dipole, a fluorophore has the greatest chance to absorb a photon. When the electric field orientation is perpendicular, there is little chance that the fluorophore will be excited. In a population of randomly oriented fluorophores, those with absorption dipole orientations similar to the electric field's orientation will be preferentially "selected" by the excitation light.

Between the absorption and the emission of a photon, the shape of a fluorophore can change. If this happens, the orientation of the absorption dipole might be different from the fluorophore's dipole orientation immediately prior to emission (the *emission dipole*). Under these conditions, it is the orientation of the emission dipole, rather than the absorption dipole, that determines the orientation of the electric field of emitted light. Obviously, if the orientations of the absorption and emission dipoles are the same (termed *collinear*), the orientation of the electric field of the emitted light can be inferred from the orientation of either dipole.

Having conveyed these basic underlying concepts of photophysics, we can now proceed to the following sections. There we will attempt to build progressively an intuitive understanding of the theory behind fluorescence polarization and anisotropy measurements, beginning with a thorough treatment of the polarization of light.

### 10.3 LIGHT HAS AN ORIENTATION

---

Time-resolved fluorescence anisotropy measurements are based on detecting a property of light resulting from the orientation of the electric field—that is, its *polarization*. Unlike other aspects of light, such as intensity and frequency, that are readily perceived by the human eye, polarization is poorly detected by humans. The intensity of light that we perceive is proportional to the number of photons detected by our eyes. The human eye can perceive changes in the intensity of light over a range of a few photons per trial to light intensities that are greater than 10 orders of magnitude brighter when gazing upon the sun on a clear day (Hecht, Schlaer, and Pirenne 1941; Inoue and Spring 1997). The human eye can also detect and discriminate between light with wavelengths ranging from about 350 to 750 nm (violet to red; Inoue and Spring 1997).

Thus, it is no surprise that we can readily and intuitively understand the meaning of a change in light intensity or color as encountered in fluorescence microscopy. As mentioned earlier, in addition to intensity and color, light also has a direction of propagation, and the electric field has an orientation in a plane perpendicular to this direction. This attribute of light is called *polarization*, which can be thought of as the orientation of the electronic oscillations of a light wave as it propagates through space. If this orientation does not change with propagation, it is called *linearly polarized light*; if the orientation does change, it can vary in a circular or an elliptical pattern. Many insects, cephalopods, and several other aquatic organisms have the ability to perceive the polarization state of light.

In contrast, human eyes have very low sensitivity to the polarization state of light and accordingly most people do not perceive differences in polarization. Humans can perceive polarization by viewing the world through a linear polarizer—a type of filter that dramatically attenuates linearly polarized light as a function of its orientation relative to the axis of the polarizer. In essence, the use of these polarizers transforms the directional orientation of light into changes in light intensity—an attribute that our eyes can readily distinguish. The use of a linear polarizer to visualize the orientation of light is illustrated in Figure 10.1. Linear polarizers can also be used to parameterize the polarization of emitted light and form the basis for building microscopes that can image changes in polarization. Before we describe how polarization is parameterized and the construction of microscopes for imaging the polarization state of light in biological samples, we first explore what happens when a population of randomly oriented fluorophores is excited by linearly polarized light.

#### 10.4 PHOTOSELECTION

---

The typical light sources used in most conventional fluorescence light microscopes (mercury arc lamps) emit light with random orientation; these sources are said to emit *natural light*. Individual photons still have polarization, but all possible orientations of photons are present in natural light.\* As a consequence, fluorophores whose absorption dipoles are in a plane perpendicular to the direction of the excitation light will have the same chance of absorbing a photon when excited using a mercury arc lamp. Thus, the emission from this population of fluorophores will also lack orientation bias if the light is observed in the direction parallel to the direction of travel of the excitation light.

This picture is very different when linearly polarized light is used to excite a population of fluorophores. Linearly polarized light can be generated by passing light with random polarization through a linear polarizer (to filter out most of the photons whose orientation does not match the orientation of the filter axis). Linearly polarized light is also produced by most of the lasers used in laser scanning microscopy. When this light is used to excite a population of randomly oriented fluorophores, not all molecules are excited with equal probability. Molecules whose absorption dipole is oriented parallel to the electric field of the light source will be preferentially excited, while molecules with absorption dipoles

---

\* These orientations are, however, constrained to the plane of polarization, which is perpendicular to the direction in which the light is traveling.

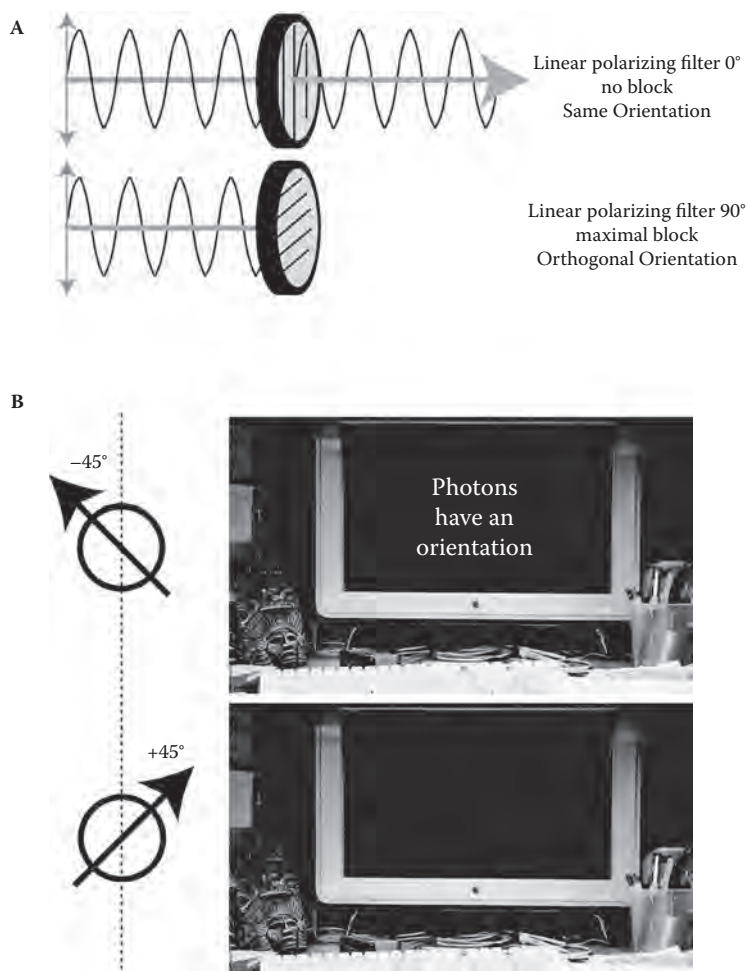


FIGURE 10.1 (See color insert following page 288). Detecting polarization. (A) The electric field of linearly polarized light is depicted as a wave orthogonal to the wave vector (green arrow). The electric field vector (blue double arrow) is also orthogonal to the wave vector and resides in a single plane for linearly polarized light. The light is transmitted if the electric field vector is parallel to the orientation of a polarizing filter (top;  $0^\circ$ ), but is attenuated if it is perpendicular (bottom;  $90^\circ$ ). (B) A digital camera was used to photograph a desktop with LCD computer monitor through a polarizing filter oriented either at  $-45^\circ$  or  $+45^\circ$  relative to the monitor's height axis. Notice how the writing displayed on the monitor is attenuated by rotating the polarizing filter by  $90^\circ$ . Also notice that the small white pilot light on the monitor casing (lower right) is not attenuated, nor are the other objects on the desk. The LCD monitor emits polarized light and therefore the intensity of its emission can be attenuated by rotation of the filter. Presumably, at  $-45^\circ$  the orientation of the polarizing filter is parallel to the electric vector of the light being emitted by the LCD monitor. In contrast, the pilot light emits natural light, and the objects on the desk primarily reflect natural light, so their image is not attenuated.

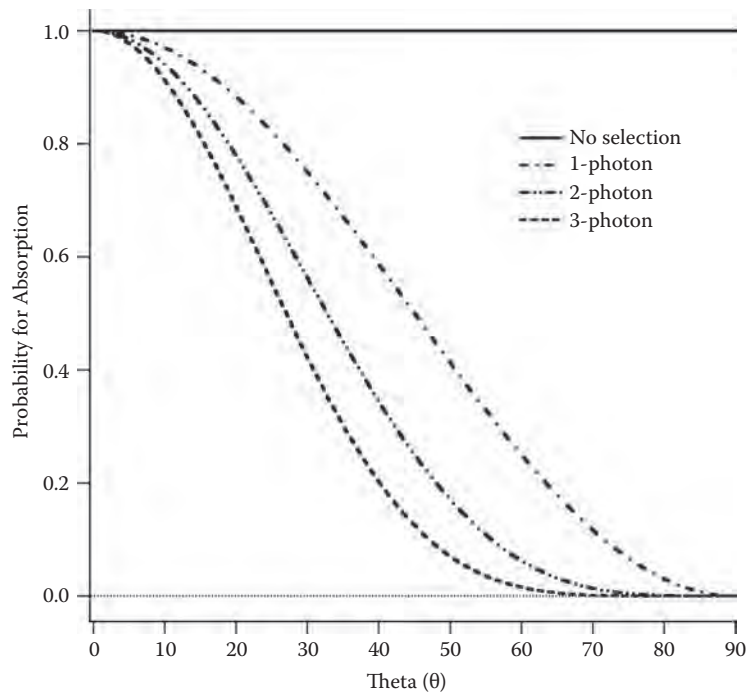


FIGURE 10.2 Fluorescence excitation with linearly polarized light. The probability of exciting a fluorophore with linearly polarized light is plotted as a function of the angle formed between the electronic vector of the excitation and the dipole orientation of the fluorophore ( $\theta$ ). This probability is also a function of the type of excitation as shown in the figure. In contrast, all fluorophores are excited with equal probability, regardless of orientation, when excited with natural unpolarized light (solid line). Note that the actual probabilities for excitation are also attenuated by the fluorophores' absorption coefficient (or multiphoton cross section and by the intensity of the excitation; not shown).

oriented exactly  $90^\circ$  to the electric field will never be excited. This excitation biased by orientation is called *photoselection* and is depicted in Figure 10.2.

A more quantitative appreciation for photoselection can be attained by considering a single fluorophore excited by linearly polarized light. For now we will assume that this fluorophore's orientation is rigid and fixed relative to the electric field of the light source. If theta ( $\theta$ ) is the angle formed between the electric field of the linearly polarized light source and the absorption dipole of a fluorophore, then the probability that a fluorophore will absorb a photon will be proportional to  $\cos^2 \theta$ . For two-photon excitation, two low-energy photons need to be absorbed almost simultaneously. Because the probability for two independent events occurring is the product of their individual probabilities, the probability for two-photon absorption will be proportional to  $\cos^4 \theta$ , and for three-photon excitation it is proportional to  $\cos^6 \theta$  (Lakowicz, Gryczynski, et al. 1992). This angular dependence of excitation is depicted in Figure 10.2. There is a sharper transition in the  $\theta$  dependence with multiphoton excitation with preferential excitation at smaller angles.

We will now consider what happens when a population of fluorophores is excited by linearly polarized light. With natural light, most of the fluorophores in a sample can be excited.\* Our objective is to understand both intuitively and quantitatively what fraction of a population of fluorophores can be excited by linearly polarized light. We shall start with a population of fluorophores that have the same absorption dipole orientation (as might be encountered in a crystal or for some hydrophobic fluorophores that partition into a membrane bilayer). If  $\theta$  is  $0^\circ$ , then the relative probability of excitation will be 1 ( $\cos^x \theta = 1$ ) for one-, two-, or three-photon excitation. All fluorophores can be excited. Obviously, the actual percentage of fluorophores that *will* get excited is also a function of their absorption coefficient (or multiphoton cross section), the excitation light intensity, and wavelength. Conversely, if  $\theta$  is exactly  $90^\circ$ , then none of the fluorophores can absorb a photon.

If, however, the population of uniformly oriented fluorophores has a  $\theta$  value between 0 and  $90^\circ$ , we will get different amounts of excitation for one-, two-, or three-photon excitation. For example, if  $\theta$  is  $45^\circ$ , then for one-photon excitation we expect a 50% probability that a fluorophore will absorb a photon ( $\cos^2(45^\circ) = 0.5$ ). With two-photon excitation, we expect that no more than 25% ( $\cos^4(45^\circ) = 0.25$ ) of the fluorophores will be excited, and with three-photon excitation the probability for excitation drops to only 12.5% ( $\cos^6(45^\circ) = 0.125$ ).

#### 10.4.1 Photoselection of a Randomly Oriented Population of Fluorophores

We now wish to consider what happens when a randomly oriented population of fluorophores is excited by linearly polarized light. What do we mean by “randomly oriented” and how do we model it both mathematically and conceptually? In the context of the defined orientation of the electric field of our polarized excitation light source, we can imagine a sphere where the electric field orientation is represented by a double arrow running through the center of the sphere and emerging out of each pole at 0 and  $180^\circ$  (see Figure 10.3). In this framework, the absorption dipole orientation of a fluorophore (relative to the electric field of the light source) is represented by a single arrow beginning at the center of the sphere and pointing to a location on the sphere’s surface (black arrow with radius  $r$ ).

All possible arrow orientations define the sphere and must have the same length in this visualization because the length of the arrow represents the dipole strength and we are modeling all orientations of the *same* dipole. In the example depicted in Figure 10.3, the angle formed between the electric field of the linearly polarized light source and the absorption dipole of a fluorophore,  $\theta$ , is  $45^\circ$ . Clearly, many other dipole orientations exist that would also have a  $\theta$  value of  $45^\circ$ ; together, this subpopulation of fluorophore orientations can be thought of as defining a *circle of latitude* (red circle in Figure 10.3).

As mentioned previously, all fluorophores that share the same  $\theta$  value (same circle of latitude) would have the same probability for excitation. Similarly, other subpopulations of fluorophores will define other circles of latitude (e.g., at  $15^\circ$ ,  $30^\circ$ , etc.) with their own unique probabilities for excitation defined by their  $\theta$  value (ranging from 0 to  $180^\circ$ ). In this

\* As previously noted, when a sample is excited with “natural light” on a microscope, the orientations of photons available for excitation is constrained to a plane that is perpendicular to the direction in which the excitation light is traveling. Thus, due to the geometry of the excitation path of light microscopes, a small subset of fluorophores with absorption dipoles oriented orthogonal to this plane will not be excited, even with “unpolarized” light.

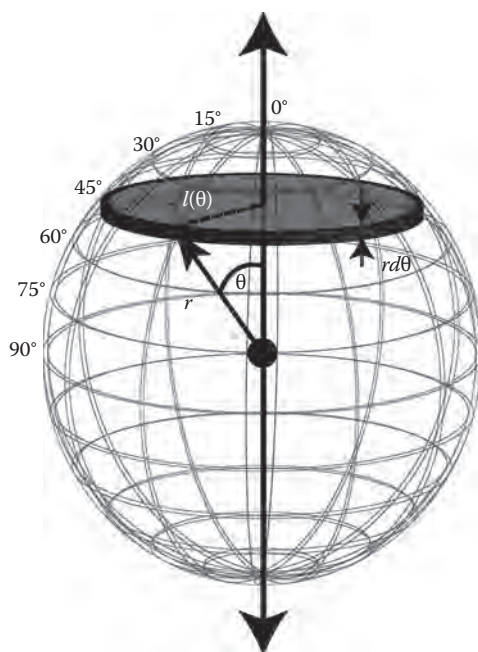


FIGURE 10.3 (See color insert following page 288). Random dipole orientation distributions. Electric field orientation is represented by a double arrow running through the center of the sphere and emerging out of each pole at 0 and 180°. The absorption dipole orientation of a fluorophore is represented by a single arrow beginning at the center of the sphere and pointing to a location on the surface of the sphere. In the example shown, the angle formed between the electric field of the linearly polarized light source and the absorption dipole of a fluorophore,  $\theta$ , is 45°. Many other dipole orientations exist that would also have a  $\theta$  value of 45° and together this subpopulation of fluorophore orientations defines a circle of latitude (red circle). All fluorophores that share the same  $\theta$  value (same circle of latitude) would have the same probability for excitation. Other subpopulations of fluorophores will define other circles of latitude (e.g., at 15°, 30°, etc.) with their own unique probabilities for excitation that are defined and parameterized by their  $\theta$  value (ranging from 0 to 90°). In this scheme, the population of all fluorophore orientations is represented by the collection of all circles of latitude, which is equivalent to the total surface area of the sphere. Accordingly, a random distribution of dipole orientations would have the same density of arrowhead distributed evenly over the entire surface of the sphere. The relative abundance of fluorophores with a specific  $\theta$  value will therefore be proportional to the surface area of its circle of latitude. This area is the product of its circumference ( $2\pi \ell$ ) times its width ( $r d\theta$ ), where  $r$  is the radius of our sphere and  $\ell$  is the radius of a circle of latitude. Note that the radius of a circle of latitude ( $\ell$ ) is itself a function of  $\theta$  ( $\ell = r \sin \theta$ ), the circumference of a circle of latitude is  $2\pi r \sin \theta$ , and its surface area will be  $2\pi r^2 \sin \theta d\theta$ . Thus, the surface area of a circle of latitude will be proportional to  $\sin \theta d\theta$ .

scheme, the population of all fluorophore orientations is represented by the collection of all circles of latitude, which is equivalent to the total surface area of the sphere. Accordingly, *a random distribution of dipole orientations would have the same density of arrowheads distributed evenly over the entire surface of the sphere.*

Next, we explore how to model this random distribution of fluorophore orientations mathematically in anticipation of calculating the distribution of fluorophores expected to be excited by linearly polarized light. Specifically, we would like to know how the number of fluorophores in a random distribution changes as a function of  $\theta$ . We might expect that, in a population of randomly oriented fluorophores, we will find the same number of fluorophores residing in each circle of latitude. That is, we will find approximately the same number of molecules with a  $\theta$  value of  $0^\circ$  as we would at  $90^\circ$ . This intuitive guess is wrong! Furthermore, the intellectual conflict generated by the failure of this hunch, we believe, is one of the main stumbling blocks toward achieving a quantitative understanding of polarization.

To understand why this distribution must be wrong we calculate the surface area defined by the area between two neighboring circles of latitude (Dill and Bromberg 2003). The surface area of two neighboring circles of latitude is simply the circumference of the circle ( $2\pi \ell$ ) times its width ( $r d\theta$ ), where  $r$  is the radius of our sphere and  $\ell$  is the radius of a circle of latitude (see Figure 10.3). Because the radius of a circle of latitude ( $\ell$ ) is itself a function of  $\theta$  ( $\ell = r \sin \theta$ ), the circumference of a circle of latitude is  $2\pi r \sin \theta$ , and its surface area will be  $2\pi r^2 \sin \theta d\theta$ . Because  $2\pi r^2$  is a constant (the value of  $r$  does not change), we see that the surface area of a circle of latitude will be proportional to  $\sin \theta d\theta$ . Thus, the surface area will be small when  $\theta$  has values close to  $0^\circ$  and it will be largest when  $\theta$  is  $90^\circ$ .

If, as proposed, the *same* number of fluorophores were to be distributed evenly over the *surface area of each differential circular area of latitude* (as the value of  $\theta$  changes), the surface density would have to decrease as the value of  $\theta$  increased from 0 to  $90^\circ$ . As mentioned earlier, the hallmark of a random distribution of fluorophore orientations is that the surface density of fluorophores will be constant over the entire surface of the sphere. To offset the influence of changing surface area, a random distribution of fluorophore orientations will occur only when the number of fluorophores found at a specific  $\theta$  value changes proportionally to the change in surface area. Specifically, for a random distribution of fluorophore orientations, the *abundance* of fluorophores having a specific  $\theta$  value must be proportional to  $\sin \theta$ . Thus, in a population of *randomly* oriented fluorophores, many more fluorophores will be oriented with  $\theta$  angles close to  $90^\circ$  than at angles close to  $0^\circ$ . A random distribution of orientations is called *isotropic*, from the Greek words *iso* (equal) and *tropos* (direction).

Starting with an isotropic distribution of fluorophores, we are now ready to calculate the distribution of fluorophores that are expected to be excited by linearly polarized light. As mentioned previously, the probability of exciting a fluorophore will be proportional to  $\cos^x \theta$ , where  $x$  is zero for excitation with natural “unpolarized” light (no photoselection), two for one-photon excitation, four for two-photon excitation, and six for three-photon excitation. With polarized light, it will be easier to excite molecules at low  $\theta$  values than at larger angles. In contrast, the probability for finding a fluorophore with a particular  $\theta$  value is proportional to  $\sin \theta$ . It will be easier to find molecules with  $\theta$  values near  $90^\circ$  than

those with values closer to  $0^\circ$ . Thus, the distribution of fluorophores that are expected to be excited by linearly polarized light (as a function of  $\theta$ ) is determined by two opposing factors and will be proportional to the product of these two factors:

$$p \propto \cos^x \theta \cdot \sin \theta \quad (10.1)$$

In Figure 10.4, the value of  $p$  is plotted as a function of  $\theta$  for excitation with natural light, and for one-, two-, and three-photon excitation with linearly polarized light. Natural light (no photoselection) has no predominant electric field orientation to serve as a fiduciary orientation ( $\theta = 0$ ) against which the orientation of excited fluorophores can be compared. Nonetheless, the distribution of fluorophore orientations excited with natural light can be considered relative to the electric field orientation of a linearly polarized light source (as would be used for one-, two-, and three-photon photoselection). Under these conditions,

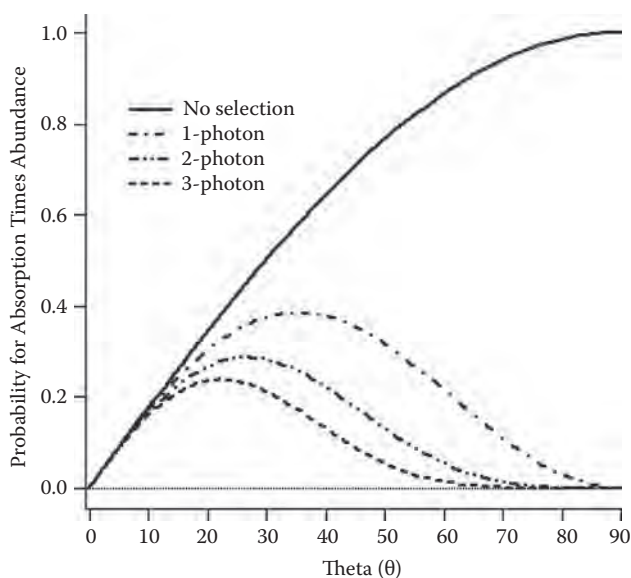


FIGURE 10.4 Photoselection with linearly polarized light. The probability of exciting a fluorophore from an isotropic population with linearly polarized light is plotted as a function of the angle formed between the electronic vector of the excitation and the dipole orientation of the fluorophore ( $\theta$ ). This probability is a function of the type of excitation as shown in the figure. Note that the shape of these curves is determined by two opposing factors, both functions of  $\theta$ ; the probability that a fluorophore will absorb a photon— $\cos^x \theta$ , where  $x$  is zero for excitation with natural light, two for excitation by one-photon excitation, four for two-photon excitation, and six for three-photon excitation; and the probability that a fluorophore will have a specific  $\theta$  value ( $\sin \theta$ ). All fluorophores are excited with equal probability, regardless of orientation, when excited with natural unpolarized light (solid line trace); thus, in this instance, the curve simply represents the relative abundance of fluorophores at different  $\theta$  value ( $\sin \theta$ ).

the distribution of fluorophore orientations excited with natural light will simply be proportional to the random orientation of the molecules in solution; most excited molecules will have an orientation with a  $\theta$  value close to  $90^\circ$  because, without photoselection, Equation 10.1 reduces to  $p \propto \sin \theta$ .

In contrast, with photoselection, the distribution of fluorophores that are excited will be skewed to lower  $\theta$  values and have modes centered at  $35^\circ$ ,  $27^\circ$ , and  $22^\circ$  for one-, two-, and three-photon excitation, respectively. Photoselection with linearly polarized light transforms an isotropic distribution of ground-state fluorophore orientations into an *anisotropic* distribution of excited fluorophores.

### 10.5 HOW DO WE DETECT POLARIZED EMISSIONS?

With the absorption of a photon, a fluorophore will be excited; from the excited state, the fluorophore will ultimately decay by a radiative or a nonradiative pathway. For simplicity, we will assume that fluorophores are immobile (they do not rotate while in the excited state) and that their absorption and emission dipole are collinear (the impact of molecular rotation and having absorption and emission dipoles that are not collinear will be discussed later). Under these conditions, the orientation of an emitted photon will be correlated with the orientation of the linearly polarized light as a result of photoselection.

Ultimately, we would like to use microscopy to follow changes in the orientation of isotropic populations of molecules to learn about their behavior and proximity to other molecules in living cells. This requires a way to parameterize and measure the orientation of emitted photons relative to the orientation of the electric vector of our linearly polarized light source. In Figure 10.5, we see a diagram depicting a transition dipole (blue double arrow) of a fluorophore (from an isotropic solution) that was excited by a linearly polarized light source (L.S.) whose electric field is shown as a black double arrow. The three-dimensional orientation of the dipole can be characterized by two angles,  $\theta$  and  $\phi$ , where  $\theta$  is the angle formed between the dipole and the X-axis in the XY-plane\* and  $\phi$  is the angle formed between the projection of the dipole on the YZ-plane (green disk) and the Z-axis.

The X-axis is parallel to the electric vector of our light source and is therefore an axis of symmetry. The Y- and Z-axes are perpendicular to the electric vector of our light source and are therefore not axes of symmetry. The light intensity emitted from our sample dipole will be proportional to the square of the dipole length, and the dipole vector can be thought of as being composed of three directional components: x, y, and z. A signal proportional to the total intensity of light emitted by our fluorophore can be measured by placing photomultiplier (P.M.) detectors on each of the three axes. The light emitted will be proportional to the sum of the three signals ( $I_{\text{total}} = I_x + I_y + I_z$ ). P.M.x will only detect light related to the yz-vector components of the dipole; x-component information is absent in this direction. Similarly, P.M.y will only detect light related to the xz-vector components, and P.M.z will only detect light related to the xy-vector components.

\* Note that although the assignment of axes' names is arbitrary, in most published treatments  $\theta$  is the angle formed between the dipole and the Z-axis. Because this chapter is describing anisotropy measurements on a light microscope, we chose to maintain the commonly accepted axes where the Z-axis projects out of the objective, and the X- and Y-axes are perpendicular to the Z-axis in the image plane.

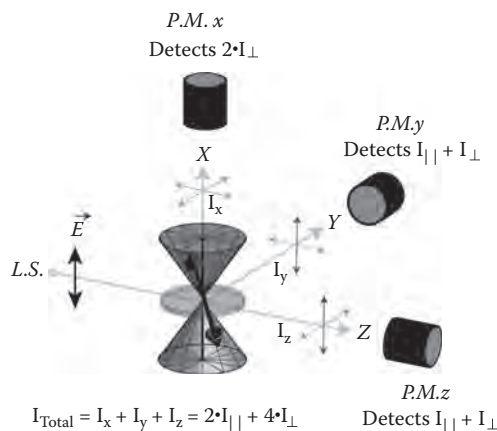


FIGURE 10.5 Detecting polarization on a microscope. The transition dipole (blue double arrow) of a fluorophore excited by a linearly polarized light source (L.S.) is shown. The electric field vector of the light source is shown as a black double arrow. The three-dimensional orientation of the dipole can be characterized by two angles,  $\theta$  and  $\phi$ , where  $\theta$  is the angle formed between the dipole and the X-axis (pink cone) and  $\phi$  is the angle formed between the projection of the dipole on the YZ-plane (green disk) and the Z-axis. The light intensity emitted from this fluorophore will be proportional to the square of the dipole strength, and the dipole vector can be thought of as being composed of three directional components: x, y, and z. A signal proportional to the total intensity of light emitted by our fluorophore can be measured summing the signals detected by photomultiplier detectors (P.M.) positioned on each of the three axes. The intensity information encoded in the x-vector component by convention is called  $I_{\parallel}$ ; the intensity information encoded in the y- and z-vector components is called  $I_{\perp}$ . As a result of photoselection and the distribution symmetry of excited molecules formed around the X-axis for an isotropic solution, the y-vector component is equal to the z-vector component. For an isotropic solution of fluorophores excited with linearly polarized light whose electric vector is parallel to the X-axis, the P.M.x detector will measure a signal whose intensity is proportional to  $2 \cdot I_{\perp}$  (see the crossed double-headed green arrows); P.M.y and P.M.z will each measure light signals whose intensity is proportional to  $I_{\parallel} + I_{\perp}$  (see the crossed double-headed red and green arrows). The total emission intensity will therefore be proportional to  $2 \cdot I_{\parallel} + 4 \cdot I_{\perp}$  or more simply  $I_{\parallel} + 2 \cdot I_{\perp}$ . Note that the xy-plane depicted here corresponds to the sample plane on a microscope, and the P.M.z detector corresponds to a photomultiplier placed after the microscope condenser (or at an equivalent position on the epifluorescence path).

The intensity information encoded in the x-vector component by convention is called  $I_{\parallel}$  and the intensity information encoded in the y- and z-vector components is called  $I_{\perp}$ . As a result of photoselection and the distribution symmetry of excited molecules formed around the X-axis for an isotropic solution, the y-vector component is equal to the z-vector component. Thus, for an isotropic solution of fluorophores excited with linearly polarized light whose electric vector is parallel to the X-axis, the P.M.x detector will measure an unpolarized light signal whose intensity is proportional to  $2 \cdot I_{\perp}$ . P.M.y and P.M.z will each

measure a polarized light signal whose intensity is proportional to  $I_{\parallel} + I_{\perp}$ . The total emission intensity will therefore be proportional to  $2 \cdot I_{\parallel} + 4 \cdot I_{\perp}$  or, more simply,  $I_{\parallel} + 2 \cdot I_{\perp}$ .

The most accessible axis available on a light microscope for measuring the polarization of emitted light from a sample is the Z-axis. As mentioned before, a photomultiplier placed along the Z-axis will collect light proportional to  $I_{\parallel} + I_{\perp}$ . Two general schemes are used to separate the  $I_{\parallel}$  signal and the  $I_{\perp}$  signal (Figure 10.6). The first arrangement measures  $I_{\parallel} + I_{\perp}$  sequentially (panels A1 and A2 in Figure 10.6), and the second arrangement measures  $I_{\parallel} + I_{\perp}$  in parallel (panel B). In the first scheme a linear polarizer (L.Pol.) is placed between the sample (S) and the light detector. A photomultiplier would typically be used for laser scanning microscopy such as confocal microscopy or two-photon microscopy and is depicted here.

The use of photomultipliers in conjunction with a pulsed laser light source allows time-resolved polarization measurements using TCSPC (Becker 2005). Essentially, two fluorescent lifetime decay curves are generated; one represents the decay of  $I_{\parallel}(t)$  and the other for  $I_{\perp}(t)$ . Alternatively, an EMCCD (electron multiplying charge-coupled device) camera would typically be used for wide-field imaging of *steady-state* polarization and for polarization imaging in TIRF (total internal reflection fluorescence) mode. When the linear polarizer is oriented at  $0^{\circ}$  relative to the electric field of the excitation source, the light detector will measure a signal proportional to  $I_{\parallel}$  (panel A1). When the polarizer is oriented at  $90^{\circ}$ , the detector will measure a signal proportional to  $I_{\perp}$  (panel A2). The orientation of the polarizing filter can be changed manually between acquisition of  $I_{\parallel}$  and  $I_{\perp}$  images; alternatively, the rotation of the polarizing filter can be mechanized using a motorized rotation stage.

Proper alignment of polarizing filters at  $0$  and  $90^{\circ}$  is key to measuring the polarization of emitted light accurately. In our laboratory, this is achieved by removing fluorescence emission filters (not depicted in Figure 10.6) from the light path (such that the linearly polarized light source projects onto the light detector directly) and then finding the rotational orientation of the polarizing filter that yields the weakest signal (by definition,  $90^{\circ}$ ). Once the  $90^{\circ}$  orientation is found, the  $0^{\circ}$  orientation is a simple  $90^{\circ}$  offset. With this calibration, precautions must be taken to prevent accidental damage to the light detector, particularly when using photomultipliers or EMCCD cameras. This can be prevented by the use of neutral density filters, low laser power settings, and low gain settings on the detector. It is worth noting that this alignment procedure assumes that the detectors are insensitive to the polarization of the light. This is not always the case; for example, side-on photomultipliers are often very sensitive to polarization while end-on tubes typically are not.

In the second scheme,  $I_{\parallel}$  and  $I_{\perp}$  signals are separated using a beam splitter and then measured in parallel (Figure 10.6, panel B). A polarizing beam splitter (Pol.B.S.) is placed after the sample to separate the  $I_{\parallel}$  fluorescent signal from the  $I_{\perp}$  signal. Typically, the  $I_{\perp}$  signal is reflected orthogonally while the  $I_{\parallel}$  signal is transmitted through the cube. It is important to note that polarizing beam splitters are wavelength dependent. Thus, it is important to choose a beam splitter that has a flat response over a broad wavelength range that is matched to the emission spectrum of the fluorophore of interest. It is also important to realize that although the *contrast ratio* (the intensity ratio of the transmitted polarization state vs. the

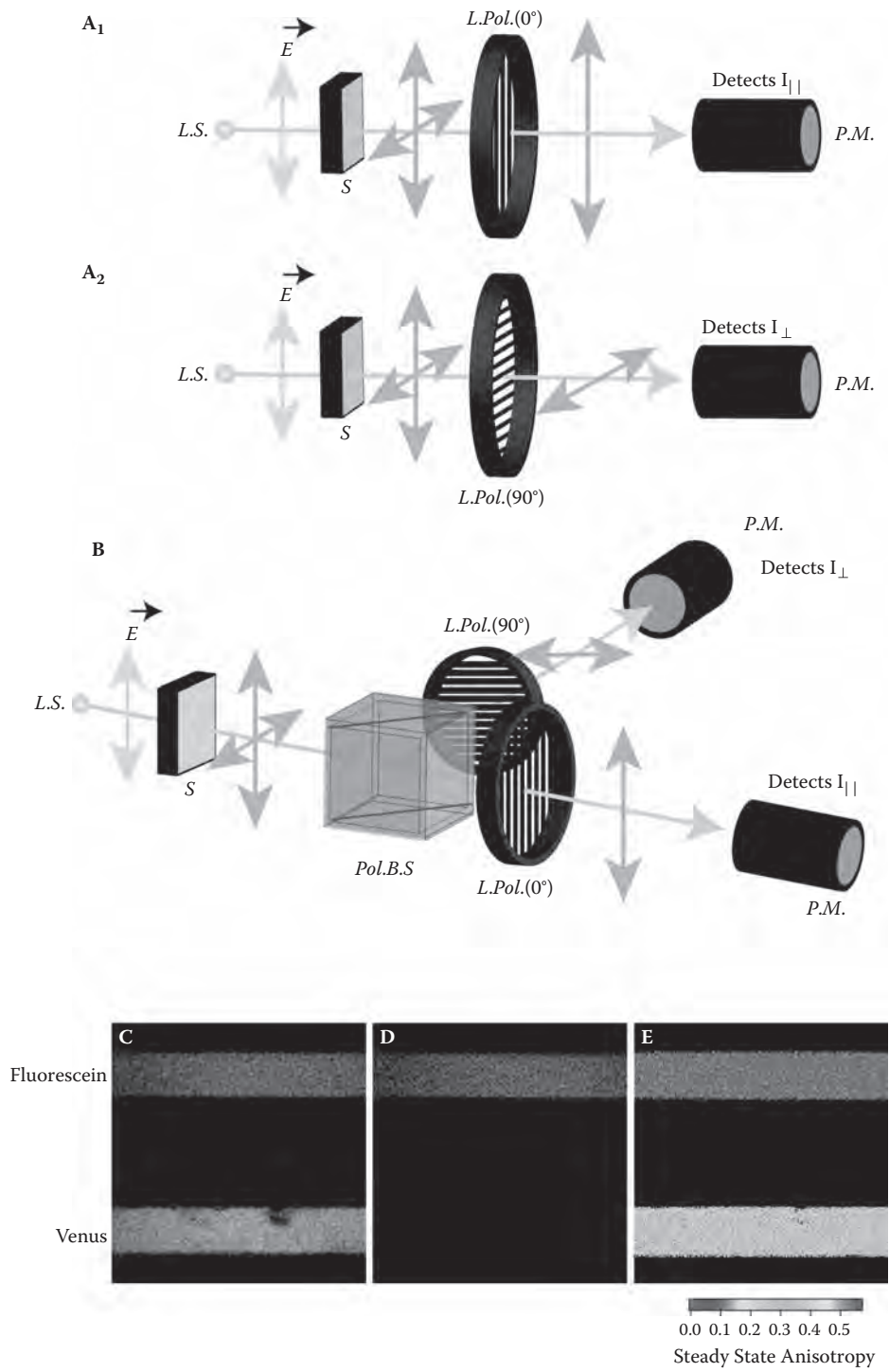


FIGURE 10.6 See caption on opposite page and see color insert following page 288.

attenuated state) of polarizing beam splitters is quite reasonable in the transmitted pathway (typically,  $\geq 500:1$ ), their performance in the reflected pathway can be poor (20:1).

For this reason, in our laboratory we augment a broadband polarizing beam splitter with two linear polarizing filters whose orientation is matched to the output of the beam splitter. Linear polarizing filters typically have contrast ratios that are at least 500:1. Higher selectivity is rarely needed because the laser outputs of most lasers used for photoselection in biological imaging applications are rarely polarized greater than 500:1. Finally, in this imaging scheme, each  $I_{\parallel}$  and  $I_{\perp}$  signal pathway has a dedicated photomultiplier.

The imaging scheme portrayed in panels A and B can also be adapted for steady-state polarization imaging (i.e., *not* time resolved). We show an example of steady-state polarization imaging (and anisotropy analysis) using a two-photon microscope configured for sequential acquisition (as depicted in panel A) in Figure 10.6(C–E). It is worth noting that the data acquisition arrangement depicted in panel B is particularly well suited for steady-state polarization imaging using cameras. Andor Technology (Belfast, Northern Ireland) manufactures a dual port camera adapter that allows two EMCCD cameras to be aligned to image  $I_{\parallel}$  and  $I_{\perp}$  in parallel. Alternatively, Cairn Research Ltd. (Faversham, UK) and MAG Biosystems (Pleasanton, California) both manufacture devices that can split an emission image into  $I_{\parallel}$  and  $I_{\perp}$  images and project them side by side onto a single EMCCD camera.

Both the sequential and parallel imaging approaches outlined in Figure 10.6 can effectively measure  $I_{\parallel}$  and  $I_{\perp}$ , but it is worth considering the pros and cons of each method. The sequential approach is simple to implement and requires only a single photodetector. This is not a very photon-efficient approach because, when  $I_{\parallel}$  data are collected,  $I_{\perp}$  data are discarded and vice versa. Furthermore, any motion occurring between acquiring  $I_{\parallel}$  and  $I_{\perp}$  images will result in pixel registration artifacts. The parallel approach is more photon efficient than the sequential approach, and it is less susceptible

**FIGURE 10.6 (See color insert following page 288.)** Separating  $I_{\parallel}$  and  $I_{\perp}$ . When a sample (S) is excited on a microscope by a linearly polarized light source (L.S.) with electronic vector E, the fluorescent emission along the z-axis (yellow arrow) will comprise  $I_{\parallel}$  and  $I_{\perp}$ . The magnitudes of these two intensity components can be measured either sequentially (panels A1 and A2) or in parallel (panel B). The sequential configuration uses a single photomultiplier (P.M.) and a linear polarizing filter (L.Pol.) that is first positioned parallel (panel A1;  $0^{\circ}$ ) to the electronic vector of the light source to measure  $I_{\parallel}$  and then perpendicular (panel A2;  $90^{\circ}$ ) to measure  $I_{\perp}$ . In the parallel detection configuration (panel B), a polarizing beam splitter (Pol.B.S.) is used in conjunction with two linear polarizing filters and two photomultipliers to measure  $I_{\parallel}$  and  $I_{\perp}$  simultaneously. Panel C: An  $I_{\parallel}$  intensity image of two capillaries filled with a solution of fluorescein (top) or Venus (bottom) acquired as in panel A1 with 950 nm two-photon excitation. Panel D: An  $I_{\perp}$  intensity image of two capillaries filled with a solution of fluorescein (top) or Venus (bottom) acquired as in panel A2 with 950 nm two-photon excitation. Panel E: A steady-state anisotropy image calculated from the  $I_{\parallel}$  and  $I_{\perp}$  images depicted in panels C and D using Equation 10.2. Note that the fluorescein capillary had a steady-state anisotropy value of 0 (blue) while the Venus capillary had a value of  $\sim 0.3$  (green). In this instance, we are using anisotropy to “image” the difference in the molecular rotation of these molecules.

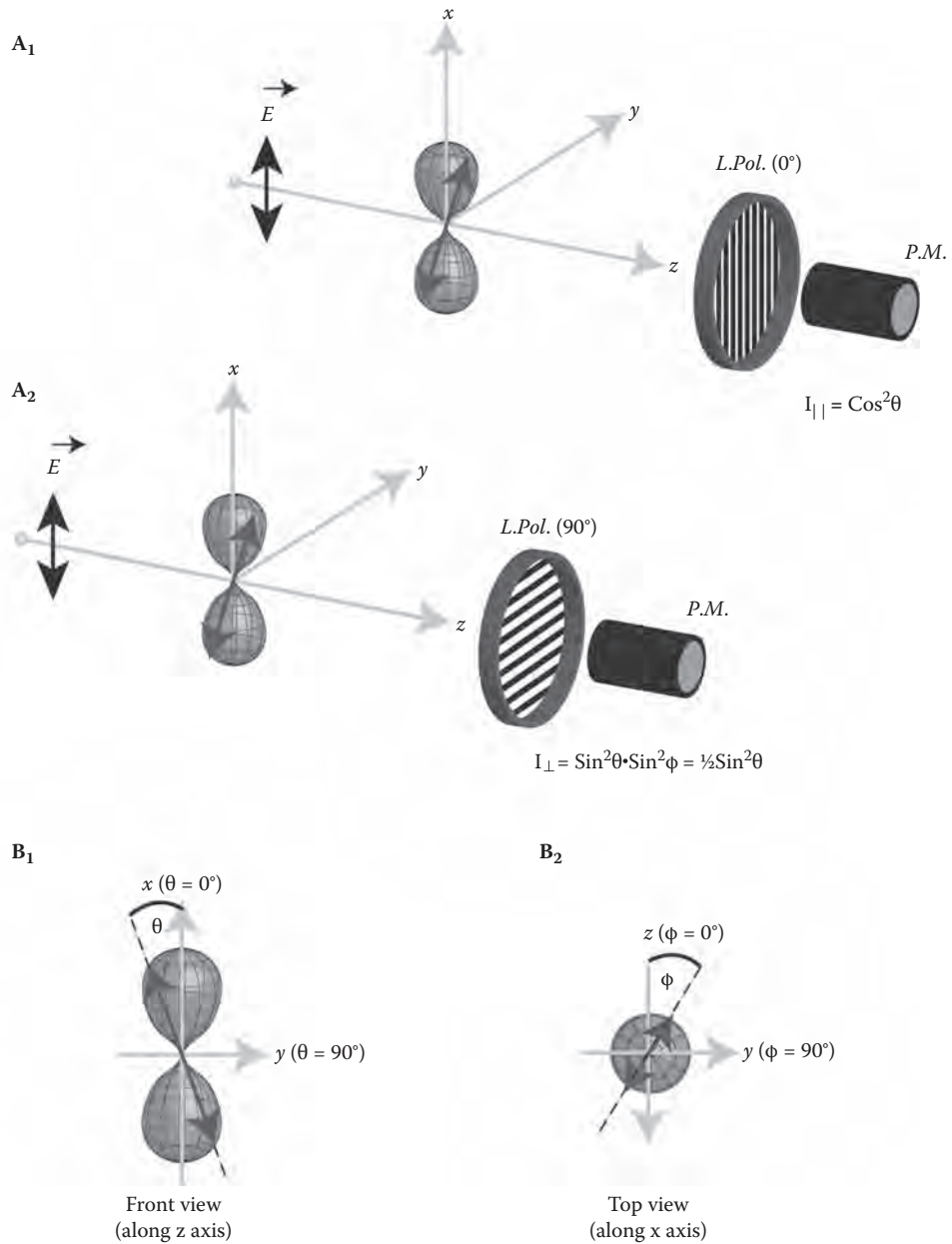


FIGURE 10.7 See caption on opposite page and see color insert following page 288.

to motion and photobleaching artifacts. This is advantageous for live cell imaging. It does, however, require two photodetectors and is therefore more expensive to implement and more difficult to align. Furthermore, the detectors might have different efficiencies for detecting photons and different instrument response functions requiring correction factors.

FIGURE 10.7 (See color insert following page 288.) The probability of detection through a polarizing filter. The probability that a photon emitted by a fluorophore will pass through a linear polarizing filter (L.Pol.) and be detected by a photomultiplier tube (P.M.) is a function of the orientation of the fluorophore's emission dipole (green double arrow) and the orientation of the filter. When the filter is situated along the z-axis and is oriented at  $0^\circ$  relative to the electric field (E) of the light source, the photomultiplier will detect  $I_{\parallel}$  (A1). When the filter is rotated to  $90^\circ$  relative to the electric field, the photomultiplier will detect  $I_{\perp}$  (A2).  $I_{\parallel}$  will be proportional to  $\cos^2\theta$ , where  $\theta$  is the angle formed between electric field of the light source and the emission dipole of the fluorophore (see panel B1).  $I_{\perp}$  will be proportional to  $\sin^2\theta \cdot \sin^2\phi$ , where  $\phi$  is the angle formed between the emission dipole of the fluorophore and the z-axis (see panel B2). For an isotropic distribution of fluorophores excited with linearly polarized light, the distribution of excited-state dipole orientations (pink hour-glass-shaped cloud) will have a symmetrical distribution of  $\phi$  values around the x-axis (B2). Due to this symmetry, the value of  $\sin^2\phi = 1/2$ . Thus, for an isotropic distribution of fluorophores  $I_{\perp}$  will be proportional to  $1/2 \sin^2\theta$ . Notice that for an isotropic population of fluorophores, the values of  $I_{\parallel}$  and  $I_{\perp}$  are functions of  $\theta$  alone.

## 10.6 HOW DO WE QUANTIFY POLARIZED EMISSIONS?

When an excited fluorophore emits a photon, the orientation of that photon's polarization will be correlated with the orientation of the fluorophore's emission dipole (Weber 1952). As mentioned previously, for a randomly oriented population of static fluorophores excited by linearly polarized light whose absorption and emission dipoles are collinear, the orientation of emitted photons will be strongly correlated with the electric field orientation of the polarized light source. Before we can understand this correlation quantitatively and apply it to biological questions we must first cover two more concepts: (1) how the orientation of a fluorophore's emission dipole affects the probability of detecting the emitted photon through either parallel or perpendicularly oriented linear polarizers, and (2) how we can use measured  $I_{\parallel}$  and  $I_{\perp}$  values to parameterize the orientation of the emission from an isotropic population of fluorophores.

In Figure 10.7, we illustrate how the orientation of an individual fluorophore's emission dipole (double green arrow) from an isotropic population of fluorophores excited with polarized light will influence the signal intensity measured through a filter polarizer oriented either parallel (A1) or perpendicular (A2) to the electric field of the light source. The three-dimensional excited-state distribution as calculated using Equation 10.1 is depicted in pink. The orientation of any single fluorophore from this excited-state population can be described by two angles:  $\theta$  (B1) and  $\phi$  (B2). When the filter polarizer is oriented to  $0^\circ$  (that is, parallel to the electric field polarization), the light intensity measured through the filter will be proportional to  $\cos^2\theta$  (where  $\theta$  is the polar angle of the emitting molecule relative to the electric field polarization).

For the population of fluorophores, the measured  $I_{\parallel}$  intensity will be proportional to an average of all the  $\cos^2\theta$  values weighted by their abundance. When the filter polarizer

is rotated to  $90^\circ$  (so that it is perpendicular to the orientation of the excitation electric field polarization), the intensity measured will be proportional to  $\sin^2 \theta \cdot \sin^2 \phi$ . Because the excited-state distribution is symmetrical around the X-axis,  $\sin^2 \phi = 1/2$ .<sup>\*</sup> Thus, for the population of fluorophores,  $I_\perp$  will be proportional to an abundance weighted average of all  $1/2 \sin^2 \theta$  values. This equation is important because it indicates that when populations of randomly oriented fluorophores are excited by linearly polarized light, the values of both  $I_\parallel$  and  $I_\perp$  will be determined by the value of  $\theta$ , the polar angle of the emitting molecules relative to the electric field polarization alone.

Finally, we must discuss how  $I_\parallel$  and  $I_\perp$  values are used to parameterize the orientation of populations of fluorophores. Two main conventions have been used in the literature: the *polarization ratio* ( $p$ ) and *emission anisotropy* ( $r$ ). The polarization ratio is simply the intensity difference between  $I_\parallel$  and  $I_\perp$  divided by the intensity observed by a photodetector placed along either the Y- or Z-axis ( $I_\parallel + I_\perp$ ; see Figure 10.5):

$$p = (I_\parallel - I_\perp)/(I_\parallel + I_\perp)$$

When  $I_\perp$  or  $I_\parallel$  is 0, the polarization ratio will have values of  $-1$  or  $1$ , respectively. This represents the full range of polarization ratio values possible with a value of  $1$  indicating a perfect alignment of emission dipoles with the orientation of the light source electric field; a value of  $-1$  indicates an orthogonal orientation. The emission anisotropy is the intensity difference between  $I_\parallel$  and  $I_\perp$  divided by an emission intensity with parallel and perpendicular components proportional to the *total* intensity ( $I_\parallel + 2 \cdot I_\perp$ ; see Figure 10.5):

$$r = (I_\parallel - I_\perp)/(I_\parallel + 2 \cdot I_\perp) \quad (10.2)$$

Now, when  $I_\perp$  or  $I_\parallel$  is 0, the emission anisotropy will have values of  $1$  to  $-0.5$ , respectively. This represents the full range of anisotropy values possible; a value of  $1$  indicates a perfect alignment of emission dipoles with the orientation of the light source and a value of  $-0.5$  indicates an orthogonal orientation of emission dipoles. It is important to realize that the polarization ratio and anisotropy are just different expressions used to parameterize the same phenomenon: the orientation of light emitted relative to the orientation of the linearly polarized light source electric field. The relationship between  $p$  and  $r$  is simply:

$$r = 2 \cdot p / (3 - p)$$

---

\* In an isotropic population of fluorophores, there is the same number of molecules with  $\phi$  values falling between  $0$  and  $180^\circ$  as between  $180$  and  $360^\circ$ . The sine function yields values between  $+1$  and  $-1$ . When the value of  $\phi$  falls between  $0$  and  $180^\circ$ ,  $\sin \phi$  has positive values, and  $\sin \phi$  has negative values when  $\phi$  has values between  $180$  and  $360^\circ$ . Thus, the average value of  $\sin \phi$  will be  $0$  (positive values cancel negatives). In contrast,  $\sin^2 \phi$  has values that fall between  $0$  and  $1$  (positive) and therefore the average value of  $\sin^2 \phi$  is  $1/2$ .

For the remainder of this chapter, we will use *emission anisotropy* because in many biological applications it is more amenable to analysis. Two important examples to illustrate this follow. First, the average anisotropy of a population of fluorophores is (Lakowicz 1999)

$$\langle r \rangle = \sum_i f_i r_i \quad (10.3)$$

where  $f_i$  is the fractional intensity and  $r_i$  is the anisotropy of a single fluorophore. This equation indicates that the *anisotropy* of a population of fluorophores is simply the intensity weighted sum of the anisotropy values of the individual fluorophores in the population.

An example that illustrates how Equation 10.3 might be useful for interpreting a biological experiment is the use of anisotropy to monitor the transition of monomers into dimers of fluorescent protein-tagged proteins upon stimulation. Prior to stimulation, the anisotropy of a population of monomers should be high because green fluorescent proteins (GFPs) rotate slowly and because Förster resonance energy transfer (FRET) does not occur with isolated fluorophores. In contrast, FRET between tagged proteins in close proximity, as might be encountered for a dimer, can result in a large decrease in anisotropy. The impact of molecular rotation and FRET on anisotropy will be discussed in detail shortly. In this type of experiment, the use of Equation 10.3 allows interpretation of intermediate anisotropy values in terms of a population comprising a mixture of monomers and dimers with different  $r$  values, whose relative abundance changes with time. Interpretation of ensemble anisotropy values from populations with more than two species of fluorophores (each having unique anisotropy values) is more problematic. Similarly, for a spherical molecule that is free to rotate and excited repeatedly with short pulses of polarized light, anisotropy will decay with time (Lakowicz 1999; Valeur 2002):

$$r(t) = r_0 \cdot e^{-t/\tau_{\text{rot}}} \quad (10.4)$$

where  $r_0$  is the *limiting anisotropy*—that is, the anisotropy measured at the instant of photo selection—and  $\tau_{\text{rot}}$  is the *rotational correlation time* of the molecule, an indicator of how rapidly a molecule rotates.

Equation 10.4 states that for an isotropic population of spherical molecules that are free to rotate, the initial anisotropy measured immediately following photoselection (at  $t = 0$ ) will be  $r_0$ , the average anisotropy value for all of the excited molecules in the population. With time, the anisotropy of this population will decay as a result of stochastic rotation until it reaches an average value of 0. If stochastic rotations occur in every axis of rotation with equal probability, the anisotropy will decay as a single-exponential function with a decay constant  $\tau_{\text{rot}}$ . Thus, by plotting the change of anisotropy as a function of time following excitation, Equation 10.4 can be used to reveal the value of the limiting anisotropy as well as the rotational correlation time.

## 10.7 THE ANISOTROPY OF RANDOMLY ORIENTED POPULATIONS OF FLUOROPHORES

What anisotropy values are expected immediately following excitation when an isotropic population of fluorophores is excited with one-, two-, or three-photon excitation using linearly polarized light? These *theoretical* values are called the *fundamental anisotropies* ( $r_f$ ; Valeur 2002). We will first explore what these values are and then discuss reasons why the *limiting anisotropy* measured in experiments is almost always less than the *fundamental anisotropy*. Figure 10.8 shows the results of a Monte Carlo simulation of an initial population of randomly oriented fluorophores (proportional to  $\sin \theta$ ). Next, fluorophores are stochastically *activated* as a function of  $\cos^x \theta$ , with  $x = 0$  for no photoselection,  $x = 2$  for one-photon excitation,  $x = 4$  for two-photon selection, and  $x = 6$  for three-photon selection (panel A). With photoselection, only a fraction of the fluorophores in the population will

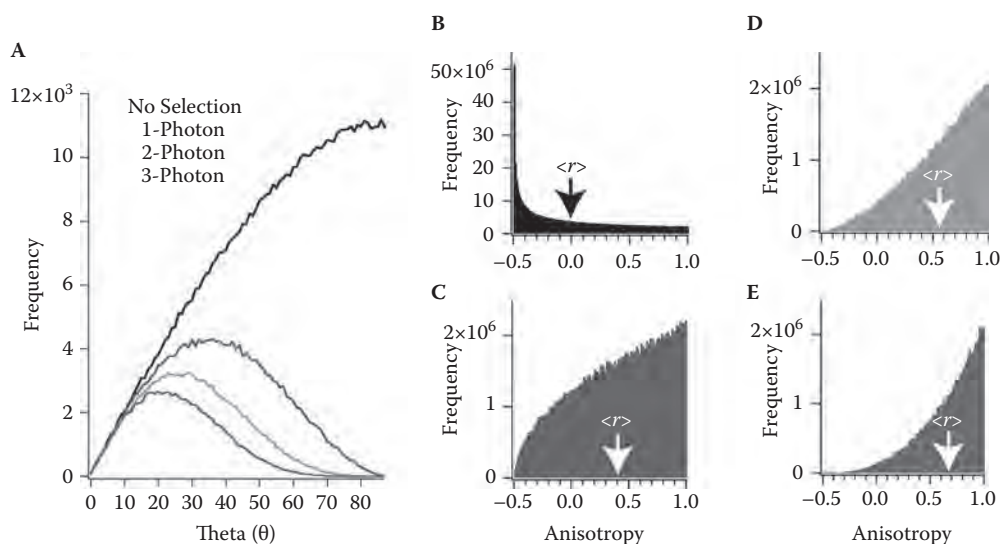


FIGURE 10.8 (See color insert following page 288.) The fundamental anisotropy value of an isotropic population. Monte Carlo simulations can be used to predict the fundamental anisotropy value of an isotropic population of fluorophores excited with natural light (panels A and B, black trace and histogram), or with one-photon (panel A and C, blue trace and histogram), two-photon (panels A and D, green trace and histogram), or three-photon (panels A and E, red trace and histogram) excitation using linearly polarized light. The distribution of theta values (A) generated by the stochastic simulation was identical to the theoretical distribution shown in Figure 10.4. Notice that the histogram of anisotropy values generated for the different excitation conditions (panels B–E) contain essentially all possible anisotropy values possible (–0.5 to 1). However, the relative abundance of these values and therefore the mean anisotropy value of the population,  $\langle r \rangle$ , are different with a value of 0 for excitation with natural light, 0.4 for one-photon excitation with polarized light, 0.57 for two-photon excitation, and 0.67 for three-photon excitation.

get excited; for example, compare the black trace (no selection, which is all molecules in all orientations excited) with the blue trace (one-photon photoselection).

For each excited fluorophore in the population, we next determine what proportion of its emitted photons will be detected by a  $I_{\parallel}$  detector, and by a  $I_{\perp}$  detector based on the individual fluorophore's  $\theta$  value. Recall that when the filter polarizer is oriented at  $0^\circ$ , the intensity measured will be proportional to  $\cos^2 \theta$  (the  $I_{\parallel}$  detector) and that when the polarizer is rotated to  $90^\circ$ , the intensity measured will be proportional to  $1/2\sin^2 \theta$  (the  $I_{\perp}$  detector). Once individual  $I_{\parallel}$  and  $I_{\perp}$  values are calculated for each activated fluorophore in a population, we next can use the  $I_{\parallel}$  and  $I_{\perp}$  values to calculate an anisotropy value for each excited fluorophore in the population using Equation 10.2. We can plot anisotropy histograms for randomly oriented populations of excited fluorophores (no selection; panel B), and those excited with one-photon photoselection (panel C), two-photon photoselection (panel D), and three-photon photoselection (panel E). These anisotropy distributions are useful for conceptualizing how the dipole orientation ( $\theta$  value) of individual excited fluorophores changes with photoselection and how this change impacts the anisotropy values measured from populations of fluorophores.

Notice that, in all four distributions, individual fluorophores with every possible anisotropy value (ranging from  $-0.5$  to  $1.0$ ) are present. Remember that the average anisotropy value is simply the intensity weighted sum of the individual anisotropy values (Equation 10.3). For excited molecules oriented randomly (no photoselection), the fundamental anisotropy (the average theoretical anisotropy value,  $r_f$ ) is  $0$ . For molecules excited by one-photon excitation,  $r_f$  is  $0.40$ ; by two-photon excitation it is  $0.57$ , and by three-photon excitation it is  $0.67$ . These values are the *fundamental anisotropy* values expected for one-, two-, and three-photon photoselection of randomly oriented populations of fluorophores (Callis 1997; Lakowicz 1999; Lakowicz, Gryczynski, et al. 1992; McClain 1972; Scott, Haber, and Albrecht 1983).

## 10.8 DEPOLARIZATION FACTORS AND SOLEILLET'S RULE

As mentioned previously, the limiting anisotropy values measured experimentally by analyzing the time-resolved decay of anisotropy using Equation 10.4 are often lower than the fundamental anisotropy values predicted by theory. Factors responsible for a decrease in the measured anisotropy are called *depolarization factors* ( $d$ ). One of the most important reasons for using anisotropy rather than polarization ratios is that the measured anisotropy is simply the fundamental anisotropy times the product of all depolarization factors (Lakowicz 1999; Valeur 2002):

$$r = r_f \cdot \prod_i d_i \quad (10.5)$$

This equation is called Soleillet's rule (Soleillet 1929). For biological experiments, typically only four depolarization factors are considered to account for a discrepancy between theory and a measured anisotropy value:

- depolarization due to the instrumentation used to measure anisotropy;
- depolarization due to noncollinear absorption and emission dipoles;
- depolarization due to molecular rotation occurring between fluorophore excitation and emission; and
- depolarization occurring as a result of FRET.

Although these depolarization factors can complicate the interpretation of anisotropy measurements, they also represent the basic reason why fluorescence anisotropy measurements are used for investigating biological processes; that is, the anisotropy measurements deliver a wealth of information about the molecular system. In the following sections, we will first illustrate how anisotropy is measured and then discuss each of these factors in greater detail.

As mentioned previously, high anisotropy values ( $I_{\parallel} > I_{\perp}$ ) indicate a strong correspondence between the orientation of the electric field vector of the excitation light and the polarization of the emitted photons. This could be observed from a population of photo-selected fluorophores whose absorption and emission dipoles are approximately collinear, have slow molecular rotation, and do not transfer energy by FRET efficiently. An anisotropy value of 0 ( $I_{\parallel} = I_{\perp}$ ) indicates that no correspondence takes place between the orientation of the electric field vector of the excitation light and the polarization of the emitted photons. This could be observed in a randomly oriented population of excited fluorophores (as a result of rapid stochastic molecular rotation or by efficient energy transfer to acceptor fluorophores with random orientations).

Negative anisotropy values ( $I_{\perp} > I_{\parallel}$ ) indicate an inverse correspondence between the orientation of the electric field vector of the excitation light and the polarization of the emitted photons as would arise if a fluorophore's absorption dipole was approximately orthogonal to its emission dipole or if efficient FRET occurs between a donor whose absorbance dipole is approximately orthogonal to the FRET acceptor's emission dipole. We have indicated that the highest anisotropy values that can be measured for a population of randomly oriented fluorophores, the *fundamental anisotropy*, is 0.4 with excitation by one-photon linearly polarized light, 0.57 with two-photon excitation, and 0.67 for three-photon excitation. In our laboratory we primarily use two-photon excitation using a mode-locked linearly polarized Ti:sapphire laser. Accordingly, the examples included here all have a fundamental anisotropy of 0.57.

In the first example, we show the decay of fluorescence from the protein Venus, a yellow spectral variant of GFP (Nagai et al. 2002), when observed by polarizers and photomultipliers positioned to observe either  $I_{\parallel}$  or  $I_{\perp}$  (Figure 10.9A, B). This pair of fluorescence lifetime decay curves was collected by TCSPC (Becker 2005) using a laser scanning microscope configured, as described in Figure 10.6(B). The sample was a HEK293 cell expressing Venus. The curves in Figure 10.9(A) depict  $I_{\parallel}(t)$  ( $\Delta$ , which are proportional to the probability of Venus emitting a photon that can pass through a linear polarizer oriented at  $0^{\circ}$ ) (parallel to the electric field polarization) as a function of time

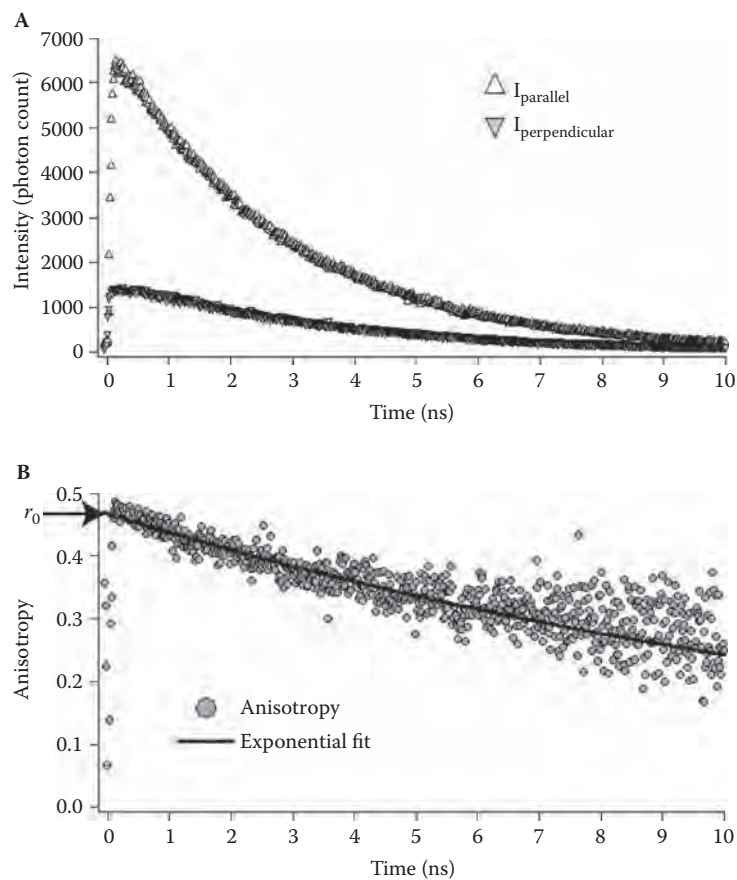


FIGURE 10.9 Anisotropy decay of Venus, a fluorescent protein. HEK cells expressing monomeric Venus were imaged using a 20X 0.5 NA water objective on a Zeiss 510 META/NLO two-photon microscope using ultrafast, 950 nm excitation pulses (at 90 MHz) from a mode-locked linearly polarized Ti:sapphire laser (Coherent). The fluorescent emission was collected through a low NA air condenser, a BG39 filter to attenuate the laser, and a  $535 \pm 15$  nm band-pass filter.  $I_{\parallel}$  and  $I_{\perp}$  were measured on a pair of MCP photomultipliers (R3809U-52; Hamamatsu) using a parallel detector anisotropy arrangement as depicted in Figure 10.6(B). Time-correlated single-photon counting was used to acquire  $I_{\parallel}(t)$  and  $I_{\perp}(t)$  lifetime decay curves (panel A;  $\Delta$  and  $\nabla$ , respectively). A Becker & Hickl SPC-830 card was used as an interface to measure timing between photodetector pulses and laser pulses. “Parallel” and “perpendicular” traces were collected in 1,024 channel histograms. Background subtraction was performed on both traces and anisotropy values calculated using Equation 10.6 yielding an anisotropy decay curve (gray circles; panel B). Solid line indicates a single-exponential fit of the anisotropy decay data using IGOR Pro (Wavemetrics). Arrow indicates the value of the limiting anisotropy,  $r_0$ .

following an ultrashort, <200 fs excitation pulse) and  $I_{\perp}(t)$   $\nabla$  (proportional to the probability of Venus emitting a photon that can pass through a linear polarizer oriented at 90°). In Figure 10.9(B), we plot the fluorescence anisotropy decay curve,  $r(t)$ , of Venus calculated from  $I_{\parallel}(t)$  and  $I_{\perp}(t)$  using a variation of Equation 10.2 that includes an experimentally measured constant,  $G$ ,\* to account for differences in the sensitivity between the two photomultipliers:

$$r(t) = [I_{\parallel}(t) - G \cdot I_{\perp}(t)] / [(I_{\parallel}(t) + 2 \cdot G \cdot I_{\perp}(t))] \quad (10.6)$$

Two features of the Venus anisotropy decay curve should be noted: the value of  $r(t)$  when  $t = 0$  and how the value  $r(t)$  changes with time. In this example, the value of  $r(t)$  when  $t = 0$  was 0.47 (see Figure 10.9B arrow). This *measured*  $t = 0$  anisotropy is the *limiting anisotropy* ( $r_0$ ). Clearly, in this example  $r_0$  is greater than the fundamental anisotropy value expected for one-photon excitation (0.4), indicating that this sample was excited by a multiphoton absorption process. The discrepancy between  $r_0$  (0.47) and the fundamental anisotropy expected for two-photon excitation (0.57) also suggests that some other process is responsible for the depolarization of our sample at  $t = 0$ . This will be explored momentarily.

Also note that during a 10 ns period following excitation and photoselection, the anisotropy value of Venus did not remain constant; that is, it did not remain at a value of 0.47. Rather, it decayed with time, and this decay can be modeled as a single exponential with a decay constant of ~15 ns (see solid line in Figure 10.9, panel B). This indicates that some additional process is responsible for the further depolarization of our sample. The depolarization factor or factors responsible for the discrepancy between our measured  $r_0$  value and the limiting anisotropy must occur on a timescale significantly faster than the time resolution of our photomultipliers (~38 ps) because they appear to occur instantaneously. In contrast, the depolarization factors responsible for the decay in anisotropy are occurring on a much slower timescale (nanoseconds).

### 10.8.1 Instrumental Depolarization

One assumption of anisotropy measurements is that the light rays forming the beam of polarized light used to excite a population of fluorophores are aligned parallel to each other. Furthermore, when the emission from a population of fluorophores is conveyed to the photodetector by way of a polarizing filter set at either 0 or 90°, the paths that the emission light rays travel should also be aligned parallel to each other and orthogonal to the surface of the polarizing filter. Although these assumptions are reasonably met when anisotropy is measured in a spectrofluorimeter, this rarely is the case when anisotropy is measured using a microscope. This is because when parallel light beams are focused by high numerical aperture (NA) lenses (such as those found in microscope objectives), the light rays no longer travel on parallel paths; rather, they converge at a focal spot (Axelrod 1979, 1989). Essentially, when anisotropy is measured using high NA optics, the lens curvature

\* The  $G$  factor for this microscope setup was measured by tail fitting of fluorescein (as described in Hess et al. 2003) and was found to be 1.26.

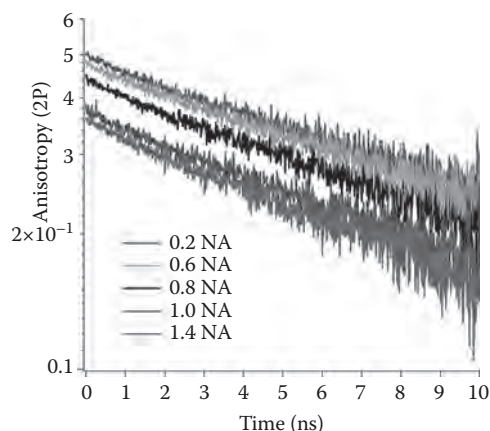


FIGURE 10.10 (See color insert following page 288.) The influence of numerical aperture on anisotropy. Purified Venus was imaged using a 10X 0.3 NA air objective on a Zeiss 510 META/NLO two-photon microscope using ultrafast, 950 nm excitation pulses (at 90 MHz) from a linearly polarized Ti:sapphire laser. The fluorescent emission of Venus was collected through an oil condenser, a BG39 filter, and a  $535 \pm 15$  nm band-pass filter. The NA of the condenser was varied from 0.2 to 1.4 by opening up the condenser aperture, and anisotropy was measured as described for Figure 10.9. As the NA of the condenser was increased, the value of  $r_0$  decreased (y-axis intercept), but the decay rate was not significantly altered. Note that the data are plotted on a semilog scale.

transforms polarized light into light composed of a mixture of electric field vector angles (elliptical polarization).

A similar process can also occur when the trajectories of polarized rays of emitted light are redirected by high NA lenses relative to the angle of a polarizing filter. The impact of this NA depolarization factor ( $d_{NA}$ ) is illustrated in Figure 10.10. In this example, linearly polarized two-photon excitation conveyed to our sample (purified Venus) through a 10X 0.3 NA objective, and the polarized emission was collected through a condenser with numerical aperture settings adjusted from 0.2 to 1.4. We see that the  $r_0$  value decreases from 0.5 to 0.36 as the NA of the condenser lens increases. Also note that despite the dramatic change in  $r_0$ , the decay rate was not significantly altered.

To maximize the dynamic range of anisotropy measurements (as well as to maximize signal-to-noise ratios), it is important to minimize depolarization due to lens curvature. Obviously, for the most accurate anisotropy measurements, the lowest NA objectives should be used. Unfortunately, low NA objectives are also the least efficient for collecting emitted photons. For live-cell imaging, photon efficiency is often an overriding concern because photons are almost always in short supply. In our laboratory, we typically use microscope optics with numerical apertures between 0.8 and 0.9 for live-cell anisotropy measurements because under these conditions,  $d_{NA} > 0.95$  (with 1 = no depolarization), the anisotropy decay kinetics are not significantly altered, and photon efficiency is not drastically compromised. It should also be noted that it is possible to use postprocessing to correct anisotropy measurement values computationally, based on the NA of the imaging system (Axelrod 1979).

### 10.8.2 Depolarization Caused by Absorption and Emission Dipole Orientation

In our previous examples, we assumed that the absorption dipole of a fluorophore was collinear with its emission dipole. We designate the angle difference between the absorption and emission dipole of a fluorophore as  $\beta$ .  $\beta$  is thought to be an intrinsic property of a specific fluorophore and should not change during the course of a biological experiment.  $\beta = 0^\circ$  for collinear fluorophores. This assumption of collinearity, however, is not always valid. Often, the absorption of a photon can cause molecular rearrangements that subtly alter the structure of the fluorophore. The depolarization factor that accounts for the relative orientation of the absorption and emission dipoles,  $d_\beta$  (Lakowicz 1999), is

$$d_\beta = \frac{3}{2} \cos^2 \beta - \frac{1}{2} \quad (10.7)$$

If  $\beta \neq 0^\circ$ , there will be a randomized offset in the orientation of emitted photons relative to the orientation of the absorption dipole. Accordingly,  $r_0$  of an isotropic solution of fluorophores will be less than the fundamental anisotropy. Assuming that the only other depolarization factor operant is  $d_{NA}$ , the predicted value of  $r_0$  using Soleillet's rule (Equation 10.5) is

$$r_0 = r_f \cdot d_{NA} \cdot d_\beta = r_f \cdot d_{NA} \cdot \left( \frac{3}{2} \cos^2 \beta - \frac{1}{2} \right) \quad (10.8)$$

Note that  $r_f$  is 2/5 (0.4) for one-photon excitation, 4/7 (0.57) for two-photon excitation, and 6/9 (0.67) for three-photon excitation. If  $d_{NA} = 1$  (no instrumental depolarization), then the measured Venus  $r_0$  value of 0.5 with two-photon excitation using low NA optics (see Figure 10.10) suggests that Venus's absorption and emission dipoles are not collinear (but see Volkmer et al. 2000) and are consistent with Venus having a  $\beta$  value of  $\sim 16^\circ$ . This number, however, is only an upper estimate because  $d_{NA}$  might have a value less than 1 (e.g.,  $\beta$  for Venus would be approximately  $13^\circ$  if  $d_{NA}$  is 0.95). Furthermore,  $\beta$  values might be different for the same fluorophore, with one-photon and multiphoton excitation as a result of different selection rules (Callis 1997; McClain 1972).

### 10.8.3 Timescale of Depolarization

Thus far we have covered two possible sources of depolarization in experiments. The first factor,  $d_{NA}$ , is a function of the instrumentation used to measure anisotropy; although it clearly affects anisotropy measurements, it tells us little about our fluorescent biological samples per se. The second depolarization factor,  $d_\beta$ , can reveal information on the structure of the fluorophore used in a biological experiment (that is, the angle between the absorption and emission dipoles), and this structural trait could potentially change as a function of the environment of the fluorophore (e.g., in different solvents). Both of these factors operate on a timescale that is significantly faster than the time resolution of most imaging systems used to measure fluorescence lifetimes or anisotropy decay (typically tens to hundreds of picoseconds). Practically speaking, they can be thought of as acting

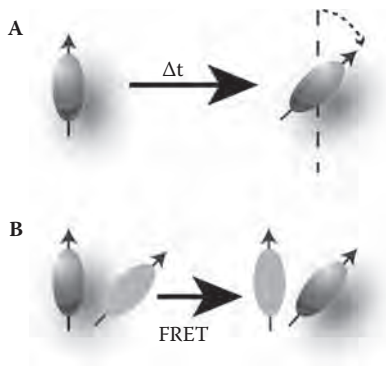


FIGURE 10.11 Two causes of depolarization on a nanosecond scale. Venus has a fluorescent lifetime of 3.4 ns and fluorescein (at pH 10) has a lifetime of 4.1 ns as measured by TCSPC-FLIM. Effectively, these fluorophores can remain in the excited state for ~16–22 ns. During this period, two types of events can result in depolarization of anisotropy measurements, molecular rotation (panel A), and FRET (panel B).

*instantaneously*. The same cannot be said for the next two depolarization factors that we will discuss: molecular rotation and FRET.

The fluorescence lifetime of a fluorophore is the average time that a fluorophore remains in the excited state. Ultimately, the fluorophore will decay to the ground state, often by emitting a photon. It is this photon that we detect and characterize in an anisotropy experiment. Most fluorophores used in biological imaging have lifetimes ranging from a few hundred picoseconds to tens of nanoseconds. For example, Venus has an average lifetime of about 3 ns, and fluorescein has an average lifetime of a little over 4 ns. This means that, following excitation by a short pulse of light, virtually every excited Venus or fluorescein molecule will decay to the ground state by five lifetimes (15–20 ns). It is useful to contemplate what events can happen within this time span, how they will affect the orientation of the fluorophore's emission dipole, and how this can be exploited for biological research. In Figure 10.11, we show the two main events (molecular rotation and FRET) that can occur within this time frame, which have the potential of altering the orientation of a fluorophore's emission dipole.

#### 10.8.4 Depolarization Caused by Molecular Rotation

If a fluorophore can freely rotate between excitation and emission (Figure 10.11A), the anisotropy signal detected for that molecule will change. With time, the biased orientation of excited fluorophores resulting from the action of photoselection with linearly polarized light will be negated by random molecular rotations. Fluorophore excitation to an excited state occurs on a femtosecond timescale ( $1 \times 10^{-15}$  s), and subsequent molecular vibration rapidly allows for the dissipation of energy as the molecule assumes the lowest vibrational energy of the  $S_1$  excited state. This process occurs on a picosecond time scale ( $1 \times 10^{-12}$  s). Molecular rotation typically is a much slower process, ranging from 10s of picoseconds to milliseconds or longer! Therefore, the longer that a fluorophore remains in the excited

state, the higher the probability is that it will rotate before emitting a photon. In essence, if molecular rotation is occurring, we expect that the anisotropy value will decay from an initial value ( $r_0$ ) to a randomized state ( $r_\infty = 0$ ).

This concept is well illustrated by observing the anisotropy decay curve of a solution of fluorescein in water in Figure 10.12. In panel A, we show  $I_{\parallel}(t)$  and  $I_{\perp}(t)$  for a solution of fluorescein. Notice that, by 1 ns after photoselection, these two intensities are identical. This means that, by 1 ns, the probability of detecting an emitted photon through a parallel oriented polarizing filter is the same as detecting it through a perpendicularly oriented filter. In panel B, we show the anisotropy decay curve calculated from  $I_{\parallel}(t)$  and  $I_{\perp}(t)$ . By 1 ns after photoselection, the anisotropy value has decayed to 0, indicating that the orientation of fluorescein's emission dipole has randomized as expected. We can model this time-dependent decrease in fluorescein's anisotropy values as a single-exponential decay (panel B, red dashed line) using Equation 10.4.

Notice that the anisotropy of fluorescein's emission decays from its initial  $r_0$  value ( $\sim 0.3$ ) to a final value of 0. With such a sharp decay, it is difficult to determine the value of  $r_0$  accurately. Also note that the value of  $r_0$  is itself a function of  $r_\beta$ ,  $d_{NA}$ , and  $d_\beta$  (see Equation 10.8). The decay constant for this fit is called the *rotational correlation time*,  $\tau_{rot}$ , and for a fluorescein solution in water has a value of 140 ps. The rotational correlation time,  $\tau_{rot}$ , is related to  $D_r$ , the *rotational diffusion coefficient*, and is a measure of how rapidly a molecule can rotate; the smaller the value of  $\tau_{rot}$  is, the faster the fluorophore can rotate. The relationship between  $\tau_{rot}$  and  $D_r$  for a small molecule in solution is (Cantor and Schimmel 1980; Lakowicz 1999):

$$\tau_{rot} = \frac{1}{6D_r} \quad (10.9)$$

Several factors can modulate the rotational correlation time because  $D_r$  is itself a function of the absolute temperature ( $T$ ), the viscosity ( $\eta$ ), and the molar volume of the fluorophore ( $V$ ) as described by the Stokes–Einstein relationship (Lakowicz 1999):

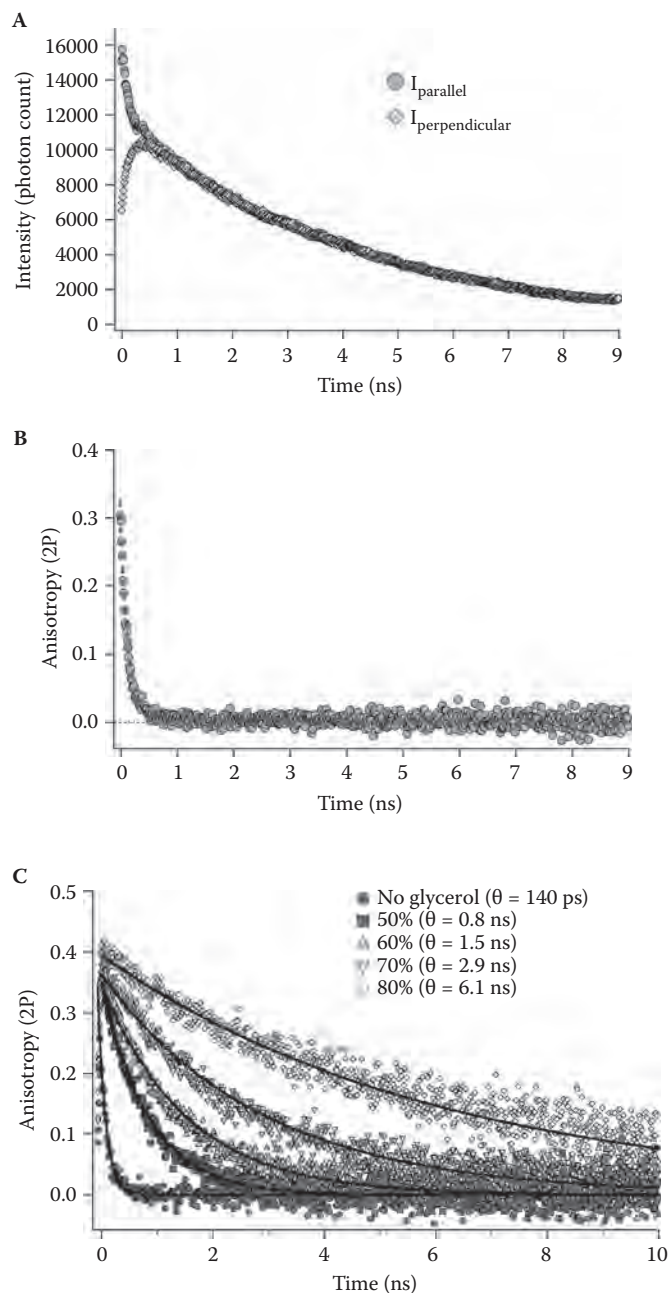
$$D_r = \frac{RT}{6V\eta} \quad (10.10)$$

where  $R$  is the gas constant. Thus,

$$\tau_{rot} = \frac{\eta V}{RT} \quad (10.11)$$

In Figure 10.12(C), we plot how the anisotropy decay of fluorescein's emission changes as the viscosity of the solution is increased by the addition of glycerol. As the solution becomes more viscous, fluorescein rotates slower and therefore it takes longer for its anisotropy to decay to 0. Notice that all five curves were well fit to a single-exponential model, but the value of  $\tau_{rot}$  increased with higher viscosity. Also notice that all five curves now appear

FIGURE 10.12 Depolarization due to rotation: the anisotropy decay of fluorescein.  $I_{\parallel}(t)$  (panel A, blue circles),  $I_{\perp}(t)$  (panel A, green diamonds), and the anisotropy decay (panel B, gray circles) of a 2.5  $\mu\text{M}$  solution of fluorescein in water was measured as described for Venus in Figure 10.9. Notice how rapidly the anisotropy decays to a value of 0. Fitting of the anisotropy decay curve to a single-exponential decay model revealed a decay constant of 140 ps (panel B, dashed line). To confirm that this value represents the rotational correlation time of fluorescein in water, we measured its decay as a function of added glycerol (to increase viscosity) while maintaining the fluorescein concentration at 2.5  $\mu\text{M}$  (panel C). Equation 10.11 predicts that as viscosity increases so does the rotational correlation time ( $\tau_{\text{rot}}$ ). Curve fitting to a single-exponential decay model (solid black lines) revealed that the decay constant became longer as the viscosity increased, consistent with an increase in the rotational correlation time.



to decay from a common origin at an anisotropy value of  $\sim 0.4$ ,  $r_0$ . It is also worth comparing the anisotropy decay curves for fluorescein in Figure 10.12(C) with the anisotropy decay curve for Venus in Figure 10.9(B). Clearly, Venus has a rotational correlation time that is much slower than that for fluorescein, even when fluorescein was placed in 80% glycerol. We have found that the rotational correlation time of Venus when expressed in HEK cells is similar to the rotational correlation time of purified Venus in 5% glycerol (data not shown).

Thus, it is unlikely that viscosity alone can explain this difference between Venus and fluorescein. The most likely explanation is that the molecular volumes of these two fluorophores are dramatically different. This is expected because fluorescein is a small molecule with a molecular weight of only 332 g/mol, and Venus is a large, 28,000 molecular weight, can-shaped protein with its fluorophore rigidly fixed inside. From a biologist's perspective, Equations 10.4 and 10.9–10.11 indicate that any factors that can change how fast a fluorophore will rotate, such as viscosity, molecular weight, hydration, molecular shape, association with other molecules, etc., can be detected using anisotropy decay analysis.

Strictly speaking, only spherically shaped fluorophores will have anisotropy values that decay as a single exponential, as described by Equation 10.4 (though this type of behavior is typically seen for small fluorophores). This is because nonspherical fluorophores will rotate at different rates along different axes. The anisotropy decay of nonspherical fluorophores is often modeled as a sum of exponentials (Lakowicz 1999):

$$r(t) = r_0 \cdot \sum_i a_i \cdot e^{-t/\tau_{rot_i}} \quad (10.12)$$

where  $a_i$  is the amplitude of each decay component.

Furthermore, in some instances (such as for some membrane dyes), fluorophores are free to rotate in some directions but not in others, thus requiring more complicated equations to model their anisotropy decay (Lakowicz 1999). It is also important to realize that anisotropy decay curves can become very complicated if multiple fluorophores are present in a sample.

It is worth noting that although anisotropy measurements are a powerful tool for measuring molecular rotation, even inside living cells, there are some obstacles to interpreting these types of experiments accurately. We will highlight three of these obstacles. First, in many biological experiments, a fluorophore is attached to a biological molecule of interest with the intention of monitoring the molecular rotation of that molecule. If the fluorophore is rigidly attached to the molecule of interest, then the orientation of that fluorophore's dipole will reflect the orientation of the molecule to which it is attached. All too often, however, the linker used to attach a fluorophore to another molecule is not rigid. Under these circumstances, the rotational component of the anisotropy decay of the fluorophore will reflect the rotational behavior of the free fluorophore as constrained by the flexibility of the linker and by the size and shape of the molecule to which the linker is attached.

Another limit to using anisotropy to measure molecular rotation results from the lifetime of the fluorophore and the time resolution of the anisotropy instrumentation. As previously mentioned, the fluorescent lifetime of a fluorophore ( $\tau$ ) is the average time that it remains in the excited state. By  $t = 5\tau$ , virtually all fluorophores have already decayed to the ground state. Furthermore, TCSPC imaging systems rarely have time resolutions that are better than 35 ps (full width at half maximum), and the  $I_{\parallel}$  and  $I_{\perp}$  lifetime decay curves will be a convolution of this instrument response function (IRF). Accordingly, anisotropy decay curves will only have data covering a time window spanning  $t = 0$  to  $5\tau$ , with a time resolution of a few 10s of

picoseconds. It is therefore difficult to measure rotational correlation times greater than  $10\tau$  or less than 10 ps *accurately*. For fluorophores like Venus and fluorescein, it will be difficult to measure rotational correlation times much larger than 30–40 ns accurately. One solution to this limitation is to use fluorophores with longer lifetimes or phosphorescence (Austin, Chan, and Jovin 1979; Dixit et al. 1982; Eads, Thomas, and Austin 1984).

A third obstacle worth considering for using anisotropy to measure molecular rotation is based on the accuracy of nonlinear fitting of multiexponential decay curves. A single-exponential decay will have at least two fitting parameters, a biexponential fit will have at least four parameters, etc. With more free fitting parameters, there is a greater possibility that there will not be a unique solution to a fit. The answer to this problem is to find ways to constrain the number of free fitting parameters. Global fitting is one such solution (Beechem, Knutson, and Brand 1986; Knutson, Beechem, and Brand 1983).

### 10.8.5 Depolarization Caused by FRET

Another source of depolarization shown in Figure 10.11 is FRET (Jablonski 1970). Förster resonance energy transfer is a physical phenomenon where the excited-state energy of a fluorophore is transferred to another molecule by a nonradiative mechanism (Förster 1948). For FRET to occur, several criteria must be met. First, the donor fluorophore and the acceptor must be in close proximity—typically less than 10 nm separating the two molecules. Second, for FRET to occur, the acceptor dipole must not be oriented perpendicular to the electric field of the donor. To transfer energy, FRET uses a dipole–dipole coupling mechanism in which the acceptor’s dipole resonates with the electric field oscillations of the donor. When the acceptor dipole is perpendicular to the electric field, it cannot “sense” the oscillations and therefore FRET does not occur.

The electric field of a donor fluorophore can be envisioned as a three dimensional *curved* wave emanating out from its oscillating dipole. Concentric field lines connecting the two poles of the dipole define equipotential surface contours of this field, and the tangent at any point on these field lines represents the direction of the electric field at that specific location. At positions close to the dipole, the curved nature of these equipotential surfaces can change dramatically, even with small changes in position. Because FRET only occurs when donor and acceptor dipoles are close to each other (within a fraction of a wavelength), the relative positions of the donor and acceptor dipoles must be accounted for. Thus, FRET will be dependent on the spatial orientation of the emission dipole of the donor and the orientation of the absorbance dipole of the acceptors, as well as on the relative positions of these dipoles in space.

This relationship between the orientation of the donor and acceptor dipoles and of their relative positions in space is called the dipole orientation factor,  $\kappa^2$  (Förster 1948). A final requirement for FRET is that there must be significant overlap between emission spectrum of a donor fluorophore and the absorption spectrum of the acceptor (Clegg 1996; Jares-Erijman and Jovin 2003; Periasamy and Day 2005; Vogel, Thaler, and Koushik 2006; Wallrabe and Periasamy 2005).

The two general types of FRET reactions, hetero-FRET and homo-FRET, differ based on spectral overlap. When the donor fluorophore and the acceptor have different absorption

and emission spectra, the transfer is called hetero-FRET. In this case, the forward FRET transfer rate (from donor to acceptor) is typically much faster than the backward rate (acceptor to donor). The basis of this difference is that there will typically be a much larger spectral overlap between the emission spectrum of the donor and the absorption spectrum of the acceptor than of the emission spectrum of the acceptor and the absorption spectrum of the donor. Therefore, in most cases, hetero-FRET can be thought of as a unidirectional transfer.

In contrast, homo-FRET (Clayton et al. 2002; Jameson, Croney, and Moens 2003) is FRET occurring between fluorophores having identical spectra. Thus, with homo-FRET the forward and backward FRET transfer rates must be the same. Unlike hetero-FRET, homo-FRET from a donor to an acceptor can immediately be transferred back again to the donor. With homo-FRET, a dynamic situation is created where energy can readily migrate back and forth between donors and acceptors; therefore, another, more descriptive name for homo-FRET is *energy migration FRET* (emFRET). Although hetero-FRET is typically measured by monitoring changes in the fluorescence intensities or lifetimes of donors and/or acceptors, theoretically there should be no net change in the intensity or lifetime of a fluorophore with emFRET (Koushik and Vogel 2008; Rizzo et al. 2004). Therefore, these classical approaches for measuring FRET normally cannot be used to monitor emFRET.

Energy migration FRET can be routinely measured using fluorescence anisotropy. This approach is based on detecting a decrease in emission polarization resulting from the transfer of excitation energy from photoselected donors to typically more randomly oriented acceptors. This approach will be described in much more detail shortly. At this point, one might naively think that using fluorescence anisotropy to monitor FRET cannot work because the dipole orientation rules dictating photoselection will be the same as the dipole orientation rules required for FRET. This is not the case. Although the efficiency of FRET is in part a function of the angle formed between absorption and emission dipoles as encoded by  $\kappa^2$ , the angular selectivity for FRET transfer is much more permissive than the angular selectivity required for photoselection itself.

Now let us consider how the fluorescence anisotropy of a static sample will be affected by emFRET. For simplicity, we assume that molecular rotation is not occurring. Photons emitted from a population of fluorophores not undergoing emFRET will all originate from directly excited fluorophores. Thus, the measured anisotropy should be equal to the limiting anisotropy. Now consider a sample that has clusters of several fluorophores in close proximity. Let  $N$  equal the number of fluorophores in a cluster that participate in emFRET. Photons emitted from a cluster of fluorophores undergoing emFRET can originate from the directly excited fluorophore that was photoselected, or they can be emitted by fluorophores residing in the same cluster that were indirectly excited by nonradiative energy migration (Berberan-Santos and Valeur 1991; Gautier et al. 2001; Tanaka and Martaga 1982; Valeur 2002). Photons emitted by the directly excited fluorophore have dipole orientations highly correlated with the orientation of the electric field vector of the excitation light source as a result of photoselection.

In contrast, the orientation of the emission dipoles of fluorophores that were indirectly excited by emFRET should have little if any correlation with the orientation of the electric

field vector of the light source. Accordingly, the anisotropy measured from fluorophore clusters should reflect the fraction of *emitters* that were directly excited and the fraction that were indirectly excited by emFRET. For example, if all of the molecules that were photoselected end up emitting, the anisotropy should be the limiting anisotropy of the fluorophore. In contrast, if all of the photons emitted were from fluorophores excited indirectly by emFRET, the anisotropy should be close to zero. Because of the additivity of anisotropy values (Equation 10.3), we expect that a population of fluorophores where half of the photons emitted come from directly excited fluorophores and half from indirectly excited fluorophores will have an anisotropy of approximately  $r_0/2$ .

It should be noted that when a fluorophore in a cluster emits, the series of energy transfer events that occurred prior to the emission are not usually known. For example, even when a fluorophore that was originally photoexcited emits, we cannot simply assume that it was excited and then emitted. An alternative possibility is that the fluorophore was photoexcited and then transferred energy to a neighbor. Next, that neighbor transferred the energy back to the original fluorophore prior to emission. In fact, much more complicated energy migration pathways are also possible involving multiple neighbors and multiple energy transfer steps before an emission event occurs. The complexity of an energy migration pathway, as well as the number of different energy transfer pathways possible (that can occur when a specific fluorophore is excited and a specific fluorophore emits) dramatically increases with the number of fluorophores in a cluster, and it can be influenced by the spatial arrangement of the fluorophores in the cluster (e.g., consider the different energy migration pathways possible between a pair of fluorophores or among six fluorophores when arranged in a row, a ring, or in a branched structure).

Due to this complexity, anisotropy measurements are not as a rule used to deduce the pathways that occur prior to an emission (though the complexity of an energy migration pathway could influence the kinetics of an anisotropy decay curve and will be mentioned shortly). More typically, anisotropy measurements are used to deduce the fraction of emission events occurring from fluorophores originally photoselected and the fraction occurring from fluorophores indirectly excited by emFRET without regard to the energy migration pathways that occurred prior to emission.

If we assume that the single-step energy transfer rate ( $\omega$ ) in a cluster of fluorophores is much greater than the emission rate of the fluorophore ( $\Gamma$ , where  $\Gamma$  is the reciprocal of the fluorescent lifetime  $\tau$ ), then as excitation energy jumps from fluorophore to fluorophore in the cluster, the probability that the fluorophore that was directly excited will emit a photon decreases with the number of fluorophores participating in emFRET in a cluster (Jameson et al. 2003; Runnels and Scarlata 1995). As a result, the fraction of directly excited emitters will decrease, and the anisotropy will drop toward zero. This provides the basis through which anisotropy can reveal the number of fluorophores engaging in energy migration.

Accordingly, the anisotropy observed for a pair of fluorophores undergoing emFRET will have an anisotropy value of approximately  $r_0/2$ , a cluster of three fluorophores undergoing emFRET will have an anisotropy value of  $\sim r_0/3$ , and a cluster of four will have an anisotropy value of  $\sim r_0/4$ . In general, if  $N$  is the number of fluorophores in a cluster participating in emFRET and  $\omega \gg \Gamma$ , then  $r \approx r_0/N$ . If  $\omega$  is not much greater than  $\Gamma$ , the anisotropy

of a complex with multiple fluorophores will have a value  $\geq r_0/N$  and can be estimated using the following equation of Runnels and Scarlata (1995) (Jameson et al. 2003):

$$r_N = r_0 \cdot \frac{1 + \omega \cdot \tau}{1 + N \cdot \omega \cdot \tau} + r_{et} \cdot \frac{(N-1) \cdot \omega \cdot \tau}{1 + N \cdot \omega \cdot \tau} \quad (10.13)$$

where

$$\omega = \frac{1}{\tau} \cdot \left( \frac{R_0}{R} \right)^6 \quad (10.14)$$

$R_0$  is the Förster distance, assuming a  $\kappa^2$  value of 2/3 (for example, 4.95 nm for Venus-to-Venus transfer);  $\tau$  is the fluorescence lifetime (for Venus  $\tau = 3.4 \pm 0.1$  ns, mean  $\pm$  SD,  $n = 6$ ; data not shown); and  $R$  is the separation distance. Essentially, when  $\omega$  is not much greater than  $\Gamma$ , a fraction of the directly excited fluorophores never transfers energy to neighbors by FRET and thus the population has a higher anisotropy value. Note that because  $r_{et}$  is small (0.016 for one-photon excitation; Berberan-Santos and Valeur 1991), the second term of Equation 10.13 can often be ignored.

As mentioned before, the molecular rotation of a fluorophore when attached to a protein can be measured by anisotropy decay analysis as a slow decay component (with a rotational correlation time  $\tau_{rot}$ ). Fluorophore rotation will also attenuate a steady-state anisotropy measurement. A variation of the Perrin equation (Perrin 1926) can be used to calculate a depolarization factor to account for this (Lakowicz 1999):

$$d_0 = \frac{1}{1 + \frac{\tau}{\tau_{rot}}} \quad (10.15)$$

Soleillet's rule (Lakowicz 1999; Soleillet 1929) for the multiplication of depolarization factors can then be used to combine the equation of Runnels and Scarlata (Equation 10.13) with the Perrin equation:

$$r = \left( r_0 \cdot \frac{1 + \omega \cdot \tau}{1 + N \cdot \omega \cdot \tau} + r_{et} \cdot \frac{(N-1) \cdot \omega \cdot \tau}{1 + N \cdot \omega \cdot \tau} \right) \cdot \frac{1}{1 + \frac{\tau}{\tau_{rot}}} \quad (10.16)$$

This equation can be used to predict steady-state anisotropy as a function of the number of fluorophores in a cluster and the rotational time constant of those fluorophores. Note that any depolarization occurring as a result of the optical design of the microscope used to measure anisotropy, as well as due to noncollinear absorption and emission dipoles, will be accounted for by measuring  $r_0$  under the same imaging conditions.

How does emFRET alter fluorescence anisotropy decay curves? *In the absence of rotation*, fluorophores directly excited will emit with anisotropy values similar to  $r_0$ . In

contrast, fluorophores excited indirectly by emFRET will typically emit with anisotropy values less than  $r_0$ . This value is  $r_{\text{et}}$ . The anisotropy value of  $r_{\text{et}}$  is a function of the dipole-dipole angle between the emFRET donor and acceptor with a value ranging between  $r_0$  and 0. When an isotropic population of fluorophores is excited by one-photon linearly polarized light, the value of  $r_{\text{et}}$  will be approximately 0.016. Upon excitation, the anisotropy of this population will decay from a value of  $r_0$  to a value of  $I \cdot r_0 + j \cdot r_{\text{et}}$ , where  $i$  and  $j$  are the fraction of directly and indirectly excited fluorophores emitting, respectively. For clusters of two fluorophores, if  $\omega \gg \Gamma$ , the value of  $i = j = 0.5$ . Thus, for dimers, the anisotropy will decay from  $r_0$  to a value of  $\sim r_0/2$ . Similarly, for trimers,  $i = 1/3$  and  $j = 2/3$ ; thus, the anisotropy will decay from  $r_0$  to a value approaching  $r_0/3$ , etc.

The kinetics of this emFRET-related anisotropy decay reflects the *net* rate of energy transfer from photoselected fluorophores to the other fluorophores in the cluster. It is important to realize that this *ensemble* transfer rate must account for back transfer to the originally excited fluorophore, but it is still proportional to the single-step emFRET transfer rates occurring within the cluster. Equation 10.14 defines the single-step energy transfer rate,  $\omega$ , from a donor to an acceptor as a function of fluorophore separation distance (again assuming that  $\kappa^2$  is 2/3). For a dimer ( $N = 2$ ), the anisotropy decay constant related to emFRET,  $\phi$ , is thought to be the following (Berberan-Santos and Valeur 1991; Gautier et al. 2001; Tanaka and Martaga 1979):

$$\phi = \frac{1}{2\omega} \quad (10.17)$$

Thus, for dimers, the anisotropy is expected to decay two times faster than the single-step emFRET transfer rate predicted by Equation 10.14. Clearly, the closer two fluorophores are, the faster the anisotropy of a dimer should decay to a value approaching  $r_0/2$ . This can be seen for constructs composed of two Venus molecules separated by 5, 17, and 32 amino acid linkers in Figure 10.13. Notice that these anisotropy decay curves are well fit with a double-exponential decay model. The slow decay components (ranged between 15.9 and 23.5 ns) were similar to the rotational correlation time observed for a single Venus molecule shown in Figure 10.9 (15 ns), and they represent the molecular rotation of the fluorescent protein when tethered to another fluorescent protein.

An interesting aspect of the photophysics of fluorescent proteins that can be exploited in anisotropy studies is their slow rotation compared to more classical fluorophores (compare the anisotropy decay curves of Venus in Figure 10.9 and fluorescein in Figure 10.12). The comparatively slow rotation of Venus results from its large size and molecular weight, and because its fluorophore is rigidly anchored within the proteins'  $\beta$ -barrel structure. Accordingly, anisotropy decay curves of fluorescent proteins when attached to other proteins should never decay faster than the rotational correlation time of the free fluorophore ( $\sim 15$  ns) unless emFRET is occurring.

In Figure 10.13, the fast decay components ( $\phi = 0.60, 0.81,$  and  $1.5$  ns for V5V, V17V, and V32V, respectively) most prominent between 0 and 2 ns are therefore interpreted as changes in the emFRET transfer rate as the separation distance between the two Venus

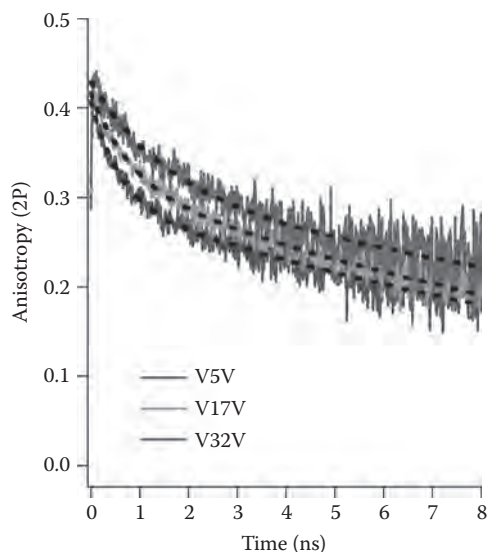


FIGURE 10.13 (See color insert following page 288.) Depolarization due to FRET: the anisotropy decay of Venus dimers. Three constructs consisting of two Venus molecules tethered to each other by 5 (V5V), 17 (V17V), and 32 (V32V) amino-acid linkers were expressed in HEK cells to demonstrate the effect of increasing the separation distance between two fluorescent proteins on anisotropy decay curves. Because these constructs are dimeric with a cluster size ( $N$ ) of two, their fast anisotropy decay components should asymptote to a value that, at most, should be half that of their limiting anisotropy. This is observed. Curve fitting with a biexponential decay model (black dashed lines) yielded a fast anisotropy decay constant ( $\phi$ ) of 0.60 ns and a slow rotational correlation time ( $\tau_{\text{rot}}$ ) of 16.3 ns for V5V; for V17V,  $\phi$  was 0.81 and  $\tau_{\text{rot}}$  was 15.9 ns and, for V32V,  $\phi$  was 1.5 and  $\tau_{\text{rot}}$  was 23.5 ns. Notice how the value of  $\phi$  increases with increased separation distance between the fluorophores.

molecules increases with linker size. Comparing this set of curves with the decay of free Venus in Figure 10.9, it should be obvious that, for fluorescent proteins with large Förster distance ( $R_0$ ; 4.95 nm for Venus-to-Venus transfer), the presence of emFRET is determined by an anisotropy decay component faster than the slow rotational component of the free fluorophore. If we now assume that  $\kappa^2$  has a value of 2/3, using a Venus fluorescence lifetime ( $\tau$ ) of 3.4 ns, we can use Equations 10.14 and 10.17 to estimate the separation distances for V5V (4.2 nm), V17V (4.4 nm), and V32V (4.9 nm). Interestingly, a hetero-FRET study of a related set of constructs (C5V, C17V, and C32V) composed of a single Cerulean acting as donor and a Venus acting as an acceptor separated by 5, 17, or 32 amino-acid linkers suggested that the separation distances between the Cerulean and Venus in those constructs were 5.7, 5.9, and 6.2 nm, respectively.

Although both sets of experiments qualitatively displayed the expected increase in FRET as the linker size was decreased, it is surprising that the separation distance measured for the Venus–Venus constructs were  $\sim 1.4$  nm shorter than the equivalent Cerulean–Venus constructs. This difference might perhaps reflect a true difference in the separation distance or dipole–dipole angle between the Cerulean–Venus and Venus–Venus constructs.

Alternatively, this discrepancy might simply reflect the difficulty of accurately measuring anisotropy decay constants by fitting multiexponential decays (having four or more free fitting parameters). Regardless, it highlights the difficulty of analyzing anisotropy decay curves *quantitatively*, and it indicates aspects of anisotropy decay analysis that need further study.

It is important to mention that the kinetics of the emFRET-related anisotropy decay components become much more complicated when the fluorophore cluster size is greater than two. Under these circumstances, the emFRET component of the anisotropy may no longer decay as a single exponential and will be dependent not only on transfer rates between fluorophores in a cluster, but also on the spatial arrangement of the fluorophores (e.g., in a row, in a ring, tetrahedron, branched, etc.). Kinetic models of the migration of energy for many of these distributions are so intractable mathematically that they are best approached using Monte Carlo simulations (Blackman et al. 1996, 1998; Marushchak and Johansson 2005). The absence of closed-form mathematical models for energy migration for various cluster arrangements is another important problem limiting our ability to use curve fitting to analyze the decay of anisotropy *quantitatively*.

Qualitatively, the amplitude of the emFRET anisotropy decay component should increase dramatically with the number of fluorophores in a cluster. This is illustrated in Figure 10.14, where the anisotropy decay curves of three fluorescent protein constructs, AAV, AVV, and VVV, are compared. In this nomenclature, V stands for Venus and A stands for Amber, a point mutation in Venus that prevents the formation of its fluorophore (Koushik et al. 2006). All three constructs should have essentially the same structure and therefore should have similar molecular rotation. AAV should have no emFRET, AVV should have an emFRET cluster size of two, and VVV should have a cluster size of three. Notice the dramatic change in the fast decay component of these anisotropy curves when comparing cluster sizes of one, two, or three Venus molecules. This change in the fast anisotropy decay component related to cluster size is much more dramatic than the subtle change observed with changes in transfer rate (Figure 10.13), and it supports the idea that the amplitude of the fast anisotropy decay component, particularly when its decay constant is significantly faster than the rotational correlation time, encodes information about cluster size.

Notice that the fast decay component of the AVV anisotropy decay curve has an asymptote that appears to be significantly less than  $r_0/2$  but that decayed faster than the rotational correlation time of AAV. The VVV curve has an asymptote that appears to be equal to  $r_0/2$  and was much less than  $r_0/3$ . This can be accounted for by Equation 10.13 if one considers that  $r_{et}$  is not equal to 0 and that  $\omega$  may not be much greater than  $\tau$ . In general, after accounting for molecular rotation, if the anisotropy drops below  $r_0/N$ , the cluster size must be greater than  $N$ .

Note, however, that the converse of this rule is not necessarily true. For example, the amplitude of the emFRET decay component of a cluster of three fluorophores might be less than  $r_0/2$  if the energy transfer rate ( $\omega$ ) is less than the emission rate of the fluorophore ( $\Gamma$ ). Under these conditions, most fluorophores will never transfer energy to a neighbor, so the vast majority of photons emitted from these clusters will be from fluorophores that were

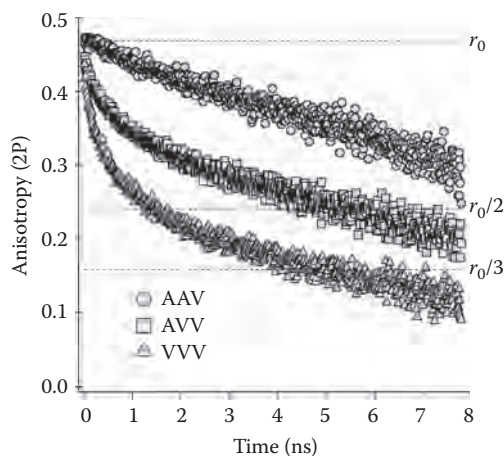


FIGURE 10.14 Depolarization due to energy migration: the impact of cluster size. Three constructs consisting of one (AAV), two (AVV), or three (VVV) Venus molecules tethered to each other and to either two (AAV), one (AVV), or zero (VVV) Amber molecules (A) were expressed in HEK cells to demonstrate the effect of cluster size ( $N$ ) on anisotropy decay curves. Amber is a single-point mutant of Venus that lacks its fluorophore and does not act as a dark absorber. AAV has a cluster size of one, AVV has a cluster size of two, and VVV has a cluster size of three. All three constructs should have approximately the same mass and shape and therefore should have similar slow rotational correlation times. Notice that all three anisotropy decay curves between 4 and 8 ns are parallel. Also notice that AAV ( $N = 1$ ) has no fast anisotropy decay component, while both AVV ( $N = 2$ ) and VVV ( $N = 3$ ) have prominent fast emFRET-related anisotropy decay components between 0 and 4 ns. The amplitude of the AVV fast decay component was significantly less than  $r_0/2$ , and the amplitude of the VVV fast component was approximately equal to  $r_0/2$ .

directly photoselected. It should be pointed out that because its amplitude would be small and its correlation time would be slow, under these circumstances, it would be very difficult to observe a “fast” emFRET anisotropy decay component, even for fluorophores like Venus that have slow rotational correlation times.

## 10.9 FLUORESCENCE ANISOTROPY APPLICATIONS

By this point it should be clear that fluorescence anisotropy measurements detect changes between the orientation of the absorption dipole of a fluorophore, as it is elevated to its excited state, and the orientation of the emission dipole of the fluorophore as it emits a photon. In the absence of energy migration, differences in anisotropy are primarily attributed to the rotation of a fluorophore while in the excited state. If energy migration can occur, depolarization can be attributed to both rotation and emFRET.

Furthermore, anisotropy can be used to measure FRET and the magnitude of the anisotropy drop can be used to determine the number of fluorophores participating in energy migration. Steady-state anisotropy measurements cannot directly differentiate between the various causes of depolarization, but time-resolved anisotropy decay analysis often can. Clearly, fluorescence anisotropy decay analysis can be used to measure molecular rotation and emFRET to reveal the rotational correlation time ( $\tau_{\text{rot}}$ ) of a fluorophore, emFRET

transfer rate ( $\omega$ ) for dimers, and cluster size ( $N$ ). In this section, we will outline three other applications of fluorescence anisotropy to illustrate other uses for these measurements in biomedical research.

### 10.9.1 Phosphorylation Assay

Anisotropy has been used to measure the binding of a phospho-specific antibody to a kinase substrate peptide (Figure 10.15; Jameson and Mocz 2005). Kinase-specific substrate peptides can be synthesized—one in the phosphorylated form and two in the dephosphorylated forms—with one having a fluorophore rigidly attached. The phosphorylated peptide is used as an antigen to generate phospho-specific antibodies. Binding specificity is determined by screening against both the phosphorylated and dephosphorylated forms of the peptide. Samples are incubated with the dephosphorylated fluorophore-tagged form of the substrate peptide.

Following incubation, samples are inactivated, and an anisotropy decay curve is acquired before and after incubation with excess antibody. Free unphosphorylated peptide should have a fast rotational correlation time (see green curve). The antibody should bind to the phosphorylated peptide during the sample incubation period. Antibody should dramatically increase the fluorophore's effective mass and therefore it should have a much slower rotational correlation time (see red decay curve in Figure 10.15). A mixture of free and bound peptide should generate a biexponential anisotropy decay curve where the amplitude of the fast rotational component indicates the fraction of free peptide (primarily unphosphorylated), and the amplitude of the slow component indicates the fraction of bound phosphorylated peptide (see blue decay curve in Figure 10.15).

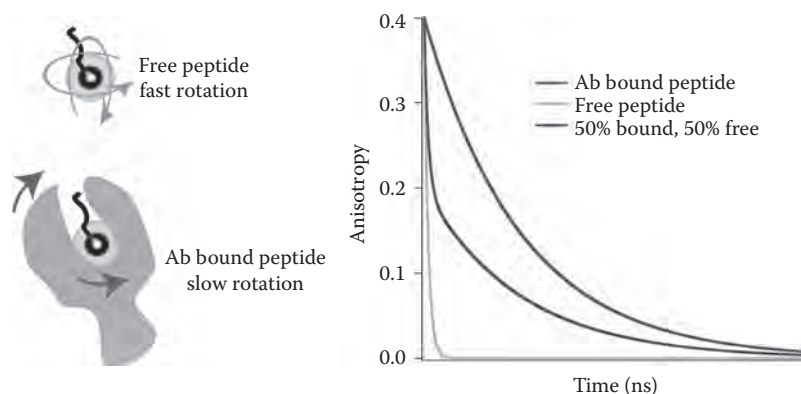


FIGURE 10.15 (See color insert following page 288). Using anisotropy to measure phosphorylation. An illustration depicting the expected anisotropy decay curve of a free fluorophore tagged short kinase substrate peptide (green trace) that can undergo fast rotations, and the curve generated by the same peptide when bound to a large antibody (upon phosphorylation; red curve). The blue decay curve depicts the biexponential decay expected from a population where 50% of the peptides are phosphorylated and bound to antibody, and 50% remain unphosphorylated and free.

10.9.2 Putting Limits on the Value of  $\kappa^2$ 

As mentioned previously, the interpretation of FRET experiments in terms of separation distances requires knowledge of the value of the dipole–dipole orientation factor,  $\kappa^2$ . This information is almost never known in biological experiments and is often assumed to have a value of 2/3 (van der Meer 2002). This assumption is appropriate if both donor and acceptor fluorophores are free to rotate in any direction at a rate that is significantly faster than their lifetimes (van der Meer 2002).

Unfortunately, this assumption may not be correct because tethering a fluorophore to a protein might hinder its rotation to some degree. Furthermore, for fluorescent proteins, this assumption is never valid (though often made) because their rotational correlation times (typically 15 ns or slower) are never faster than their lifetimes (typically ranging from 1.5 to 4 ns). Although anisotropy measurements will not reveal the actual value of  $\kappa^2$ , a comparison of the limiting anisotropy of donors and acceptors ( $r_{0\text{donor}}$ ,  $r_{0\text{acceptor}}$ , respectively) with the steady-state anisotropy values of the donors and acceptors ( $r_{\text{donor}}$ ,  $r_{\text{acceptor}}$ ) can be used to show whether these fluorophores have rotational mobility when attached to other moieties (i.e., they are not rigidly attached).

The bigger the difference is between the limiting anisotropy of a fluorophore used as a FRET donor or acceptor and the steady state anisotropy value of that fluorophore when attached to a construct, the greater their rotational freedom will be. This in turn can be used to constrain the possible values of  $\kappa^2$  in that experiment and to set ranges of probabilities to certain values in the absence of any other information. This formalism was developed by Robert Dale and Colleagues (Eisinger 1976; Dale, Eisinger, and Blumberg 1979; Eisinger and Dale 1974) and is outlined as applied by Lakowicz (1999):

$$\kappa_{\min}^2 = \frac{2}{3} \left[ 1 - \left( 0.5 \cdot \left( \sqrt{\frac{r_{\text{donor}}}{r_{0\text{donor}}}} + \sqrt{\frac{r_{\text{acceptor}}}{r_{0\text{acceptor}}}} \right) \right) \right] \quad (10.18)$$

$$\kappa_{\max}^2 = \frac{2}{3} \left[ 1 + \sqrt{\frac{r_{\text{donor}}}{r_{0\text{donor}}}} + \sqrt{\frac{r_{\text{acceptor}}}{r_{0\text{acceptor}}}} + \left( 3 \cdot \sqrt{\frac{r_{\text{donor}}}{r_{0\text{donor}}}} \cdot \sqrt{\frac{r_{\text{acceptor}}}{r_{0\text{acceptor}}}} \right) \right] \quad (10.19)$$

The limiting anisotropy values of the donor ( $r_{0\text{donor}}$ ) and acceptor ( $r_{0\text{acceptor}}$ ) are measured as the  $y$ -intercept (at  $t = 0$ ) of time-resolved anisotropy decay measurements. The steady-state anisotropy values of donor- and acceptor-tagged constructs can be calculated by pooling all photons counted by the parallel and perpendicular detectors and then using Equation 10.2. Once these limits for the value of  $\kappa^2$  have been calculated, a range of separation distances (min and max) can be calculated using the following equations:

$$R_{\min} = \sqrt[6]{\frac{\kappa_{\min}^2}{\frac{2}{3}}} \cdot \sqrt[6]{\frac{R_0^6}{E} - R_0^6} \quad (10.20)$$

$$R_{\max} = \sqrt[6]{\frac{\kappa_{\max}^2}{2/3}} \cdot \sqrt[6]{\frac{R_0^6}{E} - R_0^6} \quad (10.21)$$

where  $E$  is the FRET efficiency measured for a sample and  $R_0$  is the Förster distance for a specific donor–acceptor pair, assuming a  $\kappa^2$  value of  $2/3$ . It is important to note that the range of possible separation distances generated by this formalism is only valid if the assembly transferring energy by FRET consists of a single donor and single acceptor.

### 10.9.3 Differentiating between Directly Excited Acceptors and FRET

Hetero-FRET measurements are often acquired by exciting a sample with a wavelength optimized for the donor fluorophore while observing emission through a filter specific for the acceptor. One common problem encountered in these types of measurements is that, in addition to FRET, often a fraction of acceptors is also directly excited. The fluorescence signals from the acceptors that become excited via FRET are often weak (due to a low FRET efficiency and/or a low acceptor quantum yield); therefore, the emission of these directly excited acceptors might be interpreted as FRET, thus resulting in erroneous measurements.

Anisotropy measurements have been used to differentiate between directly excited acceptors and those excited by FRET (Piston and Rizzo 2008; Rizzo and Piston 2005). This approach is based on the idea that directly excited acceptors will have high anisotropy values and that those excited by FRET will have low anisotropy values. A sample is excited with linearly polarized light at wavelengths spanning a range covering those thought to be specific for exciting the donor and those that preferentially excite the acceptor. At each wavelength, the steady-state anisotropy is measured through a filter specific for the acceptor. The steady-state anisotropy values are plotted against excitation wavelength. If FRET is not occurring, the anisotropy will be high and will not change with excitation wavelength. If FRET is occurring, at shorter wavelengths, the anisotropy will be low; at longer excitation wavelengths, the anisotropy will be high. Intermediate anisotropy values result from a mixture of directly excited acceptors and acceptors excited by FRET.

## 10.10 CONCLUSION

Fluorescence anisotropy decay is a powerful tool for investigating molecular rotation, binding reactions, protein–protein interactions and the assembly of multimeric complexes in living cells. The inability of humans to perceive polarization and a complex theory has been a barrier to the general application of polarization-based biological imaging—specifically, anisotropy imaging. Here we have provided a simplified explanation for the theory behind this approach.

This methodology is particularly well suited for analyzing proteins tagged with spectral variants of green fluorescent protein because anisotropy decay analysis can readily differentiate between depolarization caused by rotational diffusion of this large fluorophore and energy migration FRET. We fully expect that many studies in the near future will adopt this approach to understand *in vivo* molecular assemblies because fluorescence anisotropy decay remains one of the few methods that can differentiate among monomers, dimers,

trimers, and higher order assemblies in living cells. Additional work remains, particularly in modeling anisotropy decays from more complicated fluorophore cluster geometries and from nonisotropic distributions.

## ACKNOWLEDGMENTS

This work was supported by the intramural program of the National Institutes of Health, National Institute on Alcohol Abuse and Alcoholism, Bethesda, Maryland.

## REFERENCES

- Austin, R. H., Chan, S. S., and Jovin, T. M. 1979. Rotational diffusion of cell surface components by time-resolved phosphorescence anisotropy. *Proceedings of the National Academy of Sciences USA* 76:5650–5654.
- Axelrod, D. 1979. Carbocyanine dye orientation in red cell membrane studied by microscopic fluorescence polarization. *Biophysical Journal* 26:557–573.
- Axelrod, D. 1989. Fluorescence polarization microscopy. *Methods in Cell Biology* 30:333–352.
- Bader, A. N., Hofman, E. G., van Bergen en Henegouwen, P. M. P., and Gerritsen, H. C. 2007. Imaging of protein cluster size by means of confocal time-gated fluorescence anisotropy microscopy. *Optics Express* 15:6934–6945.
- Bastiaens, P. I., and Squire, A. 1999. Fluorescence lifetime imaging microscopy: Spatial resolution of biochemical processes in the cell. *Trends in Cell Biology* 9:48–52.
- Becker, W. 2005. *Advanced time-correlated single photon counting techniques*. Berlin: Springer.
- Beechem, J. M., Knutson, J. R., and Brand, L. 1986. Global analysis of multiple dye fluorescence anisotropy experiments on proteins. *Biochemical Society Transactions* 14:832–835.
- Berberan-Santos, M. N., and Valeur, B. 1991. Fluorescence depolarization by electronic energy transfer in donor–acceptor pairs of like and unlike chromophores. *Journal of Chemical Physics* 95:8048–8054.
- Blackman, S. M., Cobb, C. E., Beth, A. H., and Piston, D. W. 1996. The orientation of eosin-5-maleimide on human erythrocyte band 3 measured by fluorescence polarization microscopy. *Biophysical Journal* 71:194–208.
- Blackman, S. M., Piston, D. W., and Beth, A. H. 1998. Oligomeric state of human erythrocyte band 3 measured by fluorescence resonance energy homotransfer. *Biophysical Journal* 75:1117–1130.
- Callis, P. R. 1997. Two-photon-induced fluorescence. *Annual Review of Physical Chemistry* 48:271–297.
- Cantor, C. R., and Schimmel, P. R. 1980. *Biophysical chemistry part II: Techniques for the study of biological structure and function*. San Francisco: W. H. Freeman & Co.
- Clayton, A. H., Hanley, Q. S., Arndt-Jovin, D. J., Subramaniam, V., and Jovin, T. M. 2002. Dynamic fluorescence anisotropy imaging microscopy in the frequency domain (rFLIM). *Biophysical Journal* 83:1631–1649.
- Clegg, R. M. 1996. Fluorescence resonance energy transfer. In *Fluorescence imaging spectroscopy and microscopy*, ed. X. F. Wang and B. Herman, 137, 179–252. Chichester, England: John Wiley & Sons, Inc.
- Clegg, R. M., Murchie, A. I., and Lilley, D. M. 1994. The solution structure of the four-way DNA junction at low-salt conditions: A fluorescence resonance energy transfer analysis. *Biophysical Journal* 66:99–109.
- Dale, R. E., and Eisinger, J. 1976. Intramolecular energy transfer and molecular conformation. *Proceedings of the National Academy of Sciences USA* 73:271–273.
- Dale, R. E., Eisinger, J., and Blumberg, W. E. 1979. The orientational freedom of molecular probes. The orientation factor in intramolecular energy transfer. *Biophysical Journal* 26:161–193.
- Denk, W., Strickler, J. H., and Webb, W. W. 1990. Two-photon laser scanning fluorescence microscopy. *Science* 248:73–76.

- Dill, K. A., and Bromberg, S. 2003. *Molecular driving forces*. New York: Garland Science.
- Dixit, B. P., Waring, A. J., Wells, K. O., III, Wong, P. S., Woodrow, G. V., III, and Vanderkooi, J. M. 1982. Rotational motion of cytochrome c derivatives bound to membranes measured by fluorescence and phosphorescence anisotropy. *European Journal of Biochemistry* 126:1–9.
- Eads, T. M., Thomas, D. D., and Austin, R. H. 1984. Microsecond rotational motions of eosin-labeled myosin measured by time-resolved anisotropy of absorption and phosphorescence. *Journal of Molecular Biology* 179:55–81.
- Eisinger, J., and Dale, R. E. 1974. Letter: Interpretation of intramolecular energy transfer experiments. *Journal of Molecular Biology* 84:643–647.
- Förster, T. 1948. Intermolecular energy migration and fluorescence. *Annalen der Physik* 2:55–75.
- Gadella, T. W. J., Jovin, T. M., and Clegg, R. M. 1993. Fluorescence lifetime imaging microscopy (FLIM): Spatial resolution of microstructures on the nanosecond time scale. *Biophysical Chemistry* 48:221–239.
- Gautier, I., Tramier, M., Durieux, C., et al. 2001. Homo-FRET microscopy in living cells to measure monomer–dimer transition of GFP-tagged proteins. *Biophysical Journal* 80:3000–3008.
- Hecht, S., Shlaer, S., and Pirenne, M. H. 1941. Energy at the threshold of vision. *Science* 93:585–587.
- Heikal, A. A., Hess, S. T., Baird, G. S., Tsien, R. Y., and Webb, W. W. 2000. Molecular spectroscopy and dynamics of intrinsically fluorescent proteins: coral red (dsRed) and yellow (Citrine). *Proceedings of the National Academy of Sciences USA* 97:11996–20001.
- Hess, S. T., Sheets, E. D., Wagenknecht-Wiesner, A., and Heikal, A. A. 2003. Quantitative analysis of the fluorescence properties of intrinsically fluorescent proteins in living cells. *Biophysical Journal* 85:2566–2580.
- Inoue, S., and Spring, K. R. 1997. *Video microscopy: The fundamentals*. New York: Plenum Press.
- Jablonski, A. 1970. Anisotropy of fluorescence of molecules excited by excitation transfer. *Acta Physiologica Pol A* 38:453–458.
- Jameson, D. M., Croney, J. C., and Moens, P. D. 2003. Fluorescence: Basic concepts, practical aspects, and some anecdotes. *Methods in Enzymology* 360:1–43.
- Jameson, D. M., and Mocz, G. 2005. Fluorescence polarization/anisotropy approaches to study protein–ligand interactions: Effects of errors and uncertainties. *Methods in Molecular Biology* 305:301–322.
- Jares-Erijman, E. A., and Jovin, T. M. 2003. FRET imaging. *Nature Biotechnology* 21:1387–1395.
- Knutson, J. R., Beechem, J. M., and Brand, L. 1983. Simultaneous analysis of multiple fluorescence decay curves: A global approach. *Chemistry and Physics Letters* 102:501–507.
- Koushik, S. V., Chen, H., Thaler, C., Puhl, H. L., III, and Vogel, S. S. 2006. Cerulean, Venus, and VenusY67C FRET reference standards. *Biophysical Journal* 91:L99–L101.
- Koushik, S. V., and Vogel, S. S. 2008. Energy migration alters the fluorescence lifetime of Cerulean: Implications for fluorescence lifetime imaging Forster resonance energy transfer measurements. *Journal of Biomedical Optics* 13:031204.
- Lakowicz, J. R. 1999. *Principles of fluorescence spectroscopy*. New York: Kluwer Academic/Plenum Publishers.
- Lakowicz, J. R., Gryczynski, I., Gryczynski, Z., Danielsen, E., and Wirth, M. J. 1992. Time-resolved fluorescence intensity and anisotropy decays of 2,5-diphenyloxzole by two-photon excitation and frequency-domain fluorometry. *Journal of Physical Chemistry* 96:3000–3006.
- Lakowicz, J. R., Szmacinski, H., Nowaczyk, K., Berndt, K. W., and Johnson, M. 1992. Fluorescence lifetime imaging. *Analytical Biochemistry* 202:316–330.
- Marushchak, D., and Johansson, L. B. 2005. On the quantitative treatment of donor–donor energy migration in regularly aggregated proteins. *Journal of Fluorescence* 15:797–803.
- McClain, W. M. 1972. Polarization dependence of three-photon phenomena for randomly oriented molecules. *Journal of Chemical Physics* 57:2264–2272.

- Nagai, T., Ibata, K., Park, E. S., Kubota, M., Mikoshiba, K., and Miyawaki, A. 2002. A variant of yellow fluorescent protein with fast and efficient maturation for cell-biological applications. *Nature Biotechnology* 20:87–90.
- Periasamy, A., and Day, R. N., eds. 2005. *Molecular imaging: FRET microscopy and spectroscopy*. New York: Oxford University Press.
- Perrin, F. 1926. Polarization de la lumiere de fluorescence: Vie moyenne des molecules dans l'etat excite. *Journal de Physique et le Radium V* 7:390–401.
- Piston, D. W., and Rizzo, M. A. 2008. FRET by fluorescence polarization microscopy. *Methods in Cell Biology* 85:415–430.
- Rao, M., and Mayor, S. 2005. Use of Forster's resonance energy transfer microscopy to study lipid rafts. *Biochimica et Biophysica Acta* 1746:221–233.
- Rizzo, M. A., and Piston, D. W. 2005. High-contrast imaging of fluorescent protein FRET by fluorescence polarization microscopy. *Biophysical Journal* 88:L14–16.
- Rizzo, M. A., Springer, G. H., Granada, B., and Piston, D. W. 2004. An improved cyan fluorescent protein variant useful for FRET. *Nature Biotechnology* 22:445–449.
- Runnels, L. W., and Scarlata, S. F. 1995. Theory and application of fluorescence homotransfer to melittin oligomerization. *Biophysical Journal* 69:1569–1583.
- Scott, T. W., Haber, K. S., and Albrecht, A. C. 1983. Two-photon photoselection in rigid solutions: A study of the B2u → A1g transition in benzene. *Journal of Chemical Physics* 78:150–157.
- Sharma, P., Varma, R., Sarasij, R. C., Ira, Gousset, K., Krishnamoorthy, G., et al. 2004. Nanoscale organization of multiple GPI-anchored proteins in living cell membranes. *Cell* 116:577–589.
- Soleillet, P. 1929. Sur les parametres caracterisant la polarisation partielle de la lumiere dans les phenomenes de fluorescence. *Annales de Physique (Paris)* 12:23–97.
- Suhling, K., Siegel, J., Lanigan, P. M., Leveque-Fort, S., Webb, S. E., Phillips, D., et al. 2004. Time-resolved fluorescence anisotropy imaging applied to live cells. *Optics Letters* 29:584–586.
- Tanaka, F., and Martaga, N. 1979. Theory of time-dependent photo-selection in interacting fixed systems. *Photochemistry and Photobiology* 29:1091–1097.
- Tanaka, F., and Martaga, N. 1982. Dynamic depolarization of interacting fluorophores. Effect of internal rotation and energy transfer. *Biophysical Journal* 39:129–140.
- Thaler, C., Koushik, S. V., Puhl, H. L., Blank, P. S., and Vogel, S. S. 2009. Structural rearrangement of CaMKIIa catalytic domains encodes activation. *Proceedings of the National Academy of Sciences USA* 10.1073/pnas.0901913106.
- Valeur, B. 2002. *Molecular fluorescence*. Weinheim: Wiley-VCH.
- van der Meer, B. W. 2002. Kappa-squared: From nuisance to new sense. *Journal of Biotechnology* 82:181–196.
- Varma, R., and Mayor, S. 1998. GPI-anchored proteins are organized in submicron domains at the cell surface. *Nature* 394:798–801.
- Vogel, S. S., Thaler, C., and Koushik, S. V. 2006. Fanciful FRET. *Sci STKE* 2006: re2.
- Volkmer, A., Subramaniam, V., Birch, D. J., and Jovin, T. M. 2000. One- and two-photon excited fluorescence lifetimes and anisotropy decays of green fluorescent proteins. *Biophysical Journal* 78:1589–1598.
- Wallrabe, H., and Periasamy, A. 2005. Imaging protein molecules using FRET and FLIM microscopy. *Current Opinion in Biotechnology* 16:19–27.
- Wang, X. F., Periasamy, A., and Herman, B. 1992. Fluorescence lifetime imaging microscopy (FLIM): Instrumentation and applications. *Critical Reviews in Analytical Chemistry* 23:369–395.
- Weber, G. 1952. Polarization of the fluorescence of macromolecules. I. Theory and experimental method. *Biochemical Journal* 51:145–155.
- Yan, Y., and Marriott, G. 2003. Fluorescence resonance energy transfer imaging microscopy and fluorescence polarization imaging microscopy. *Methods in Enzymology* 360:561–580.
- Yeow, E. K., and Clayton, A. H. 2007. Enumeration of oligomerization states of membrane proteins in living cells by homo-FRET spectroscopy and microscopy: Theory and application. *Biophysical Journal* 92:3098–3104.

Reference:

Chapter 10: Time Resolved Fluorescence Anisotropy. S.S. Vogel, C. Thaler, P.S. Blank, and S.V. Koushik in **FLIM Microscopy in Biology and Medicine**, pages 245-290, Boca Raton: Taylor & Francis (2009).

Figure 1

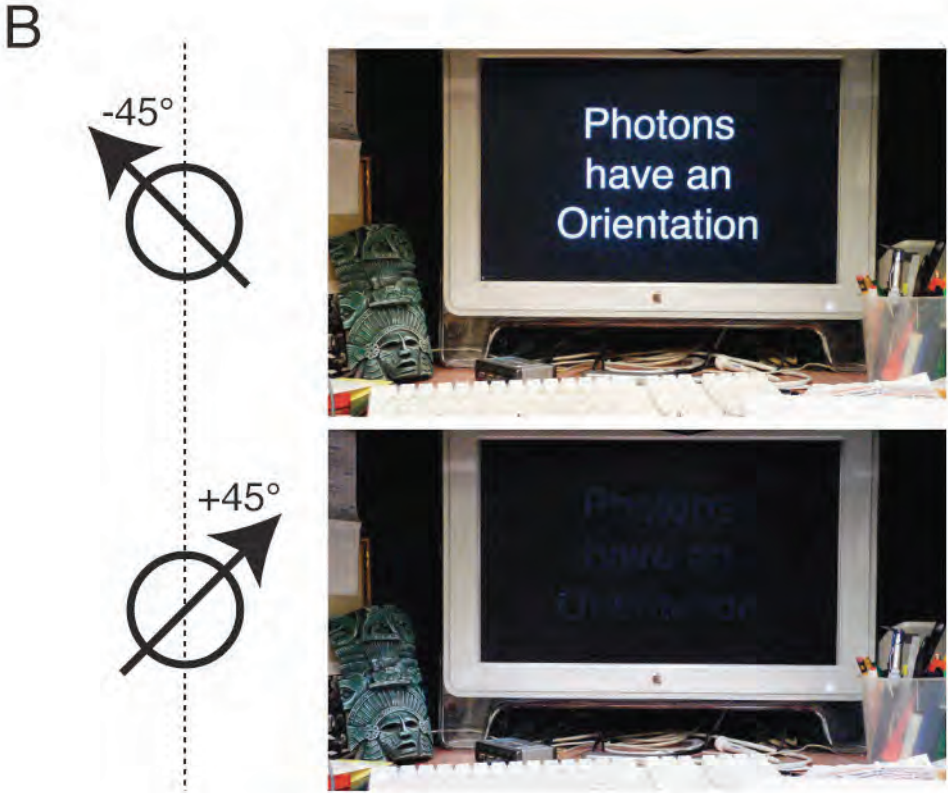
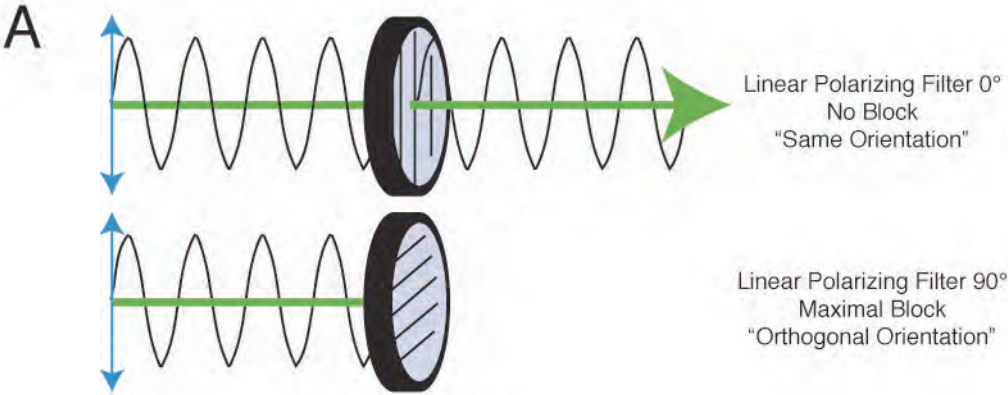


Figure 2

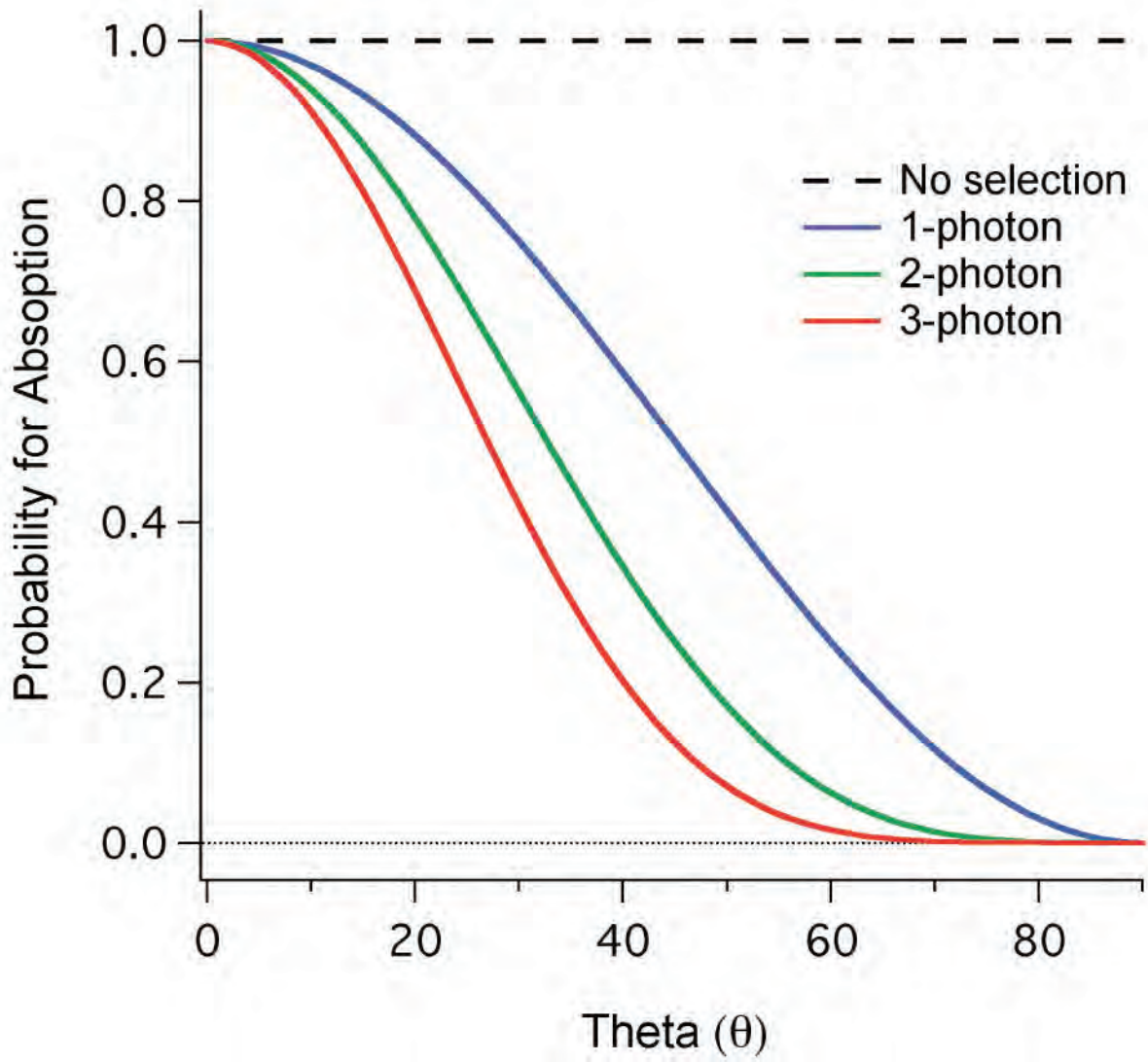


Figure 3

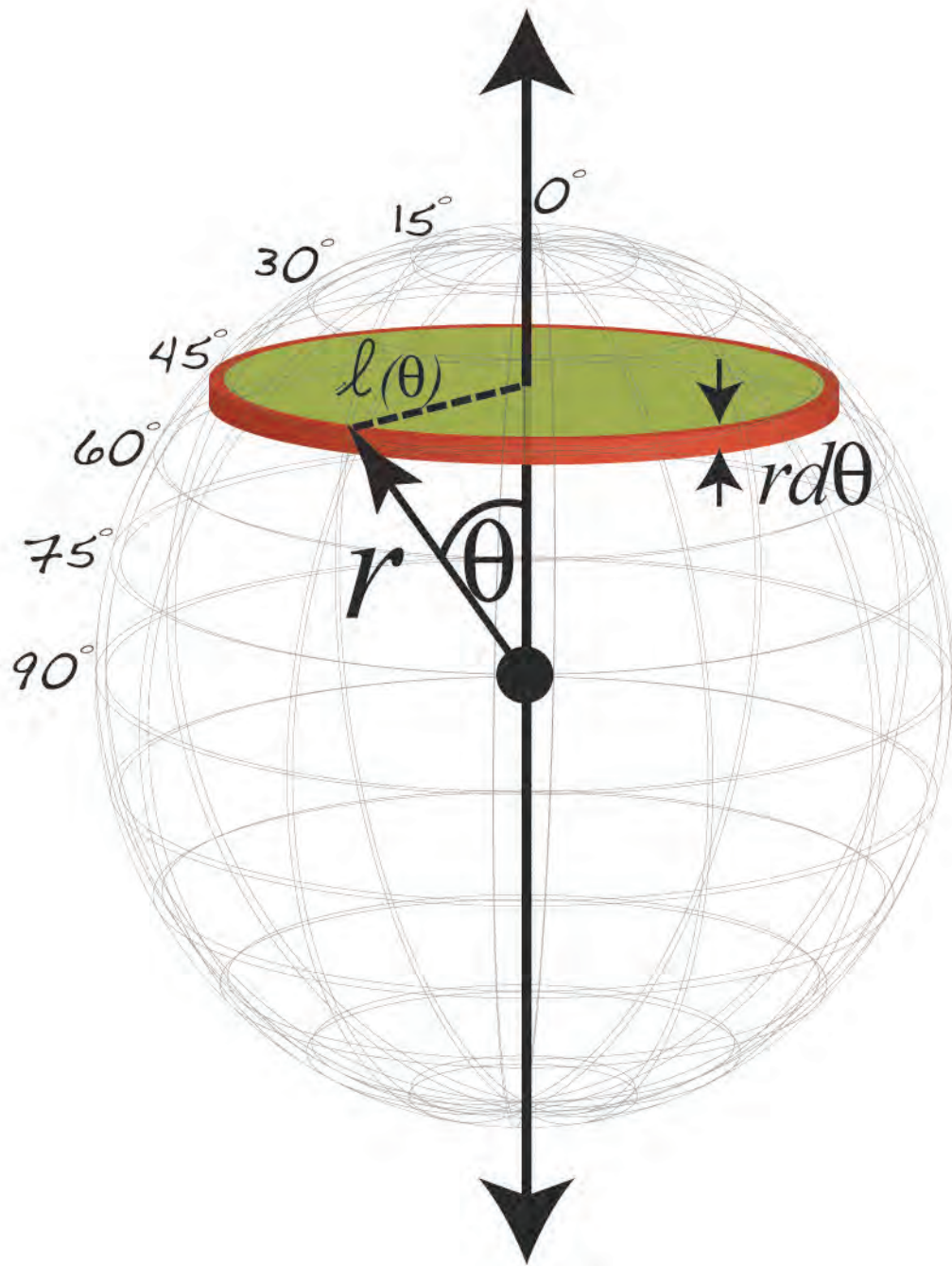


Figure 4

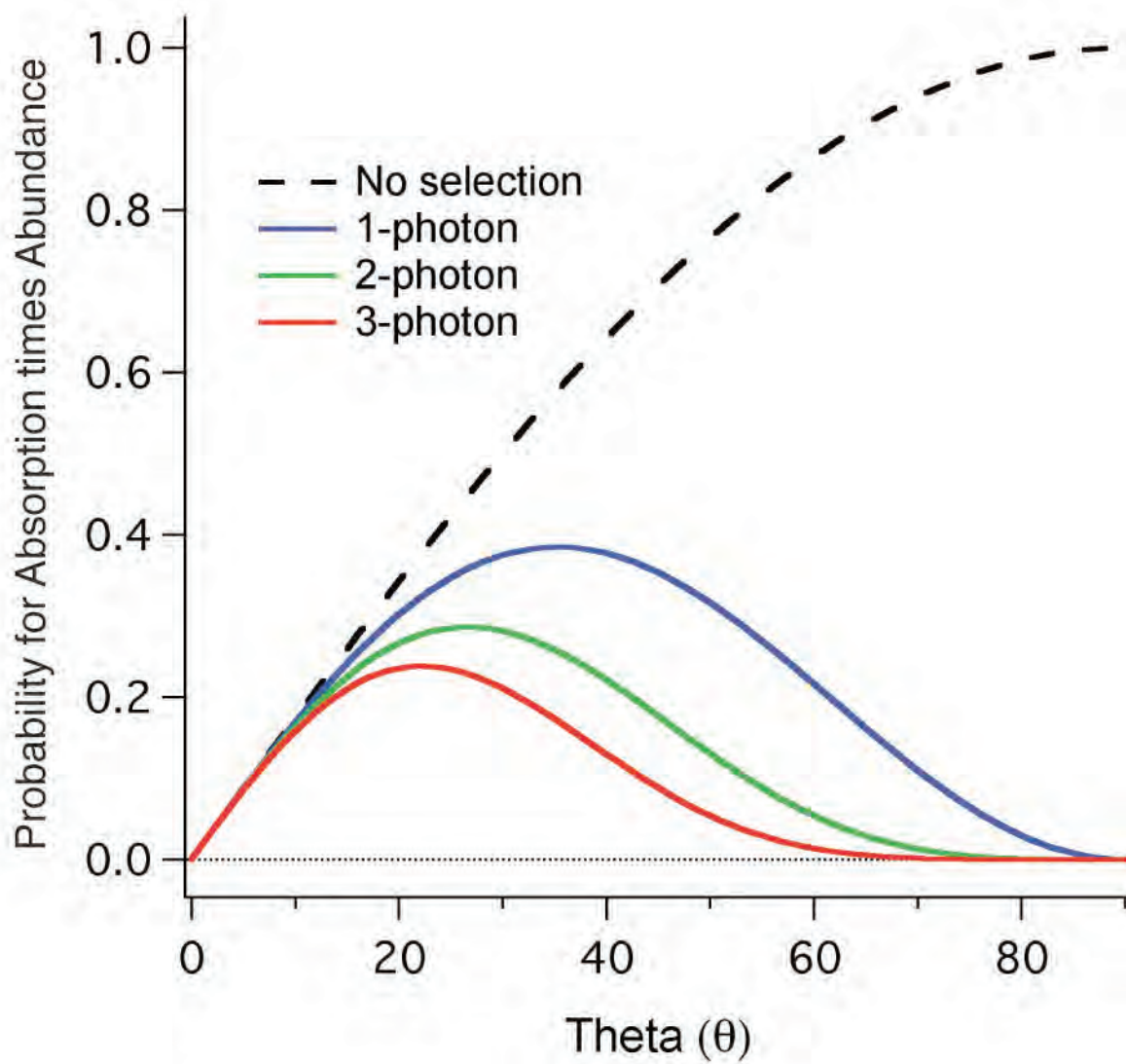


Figure 5

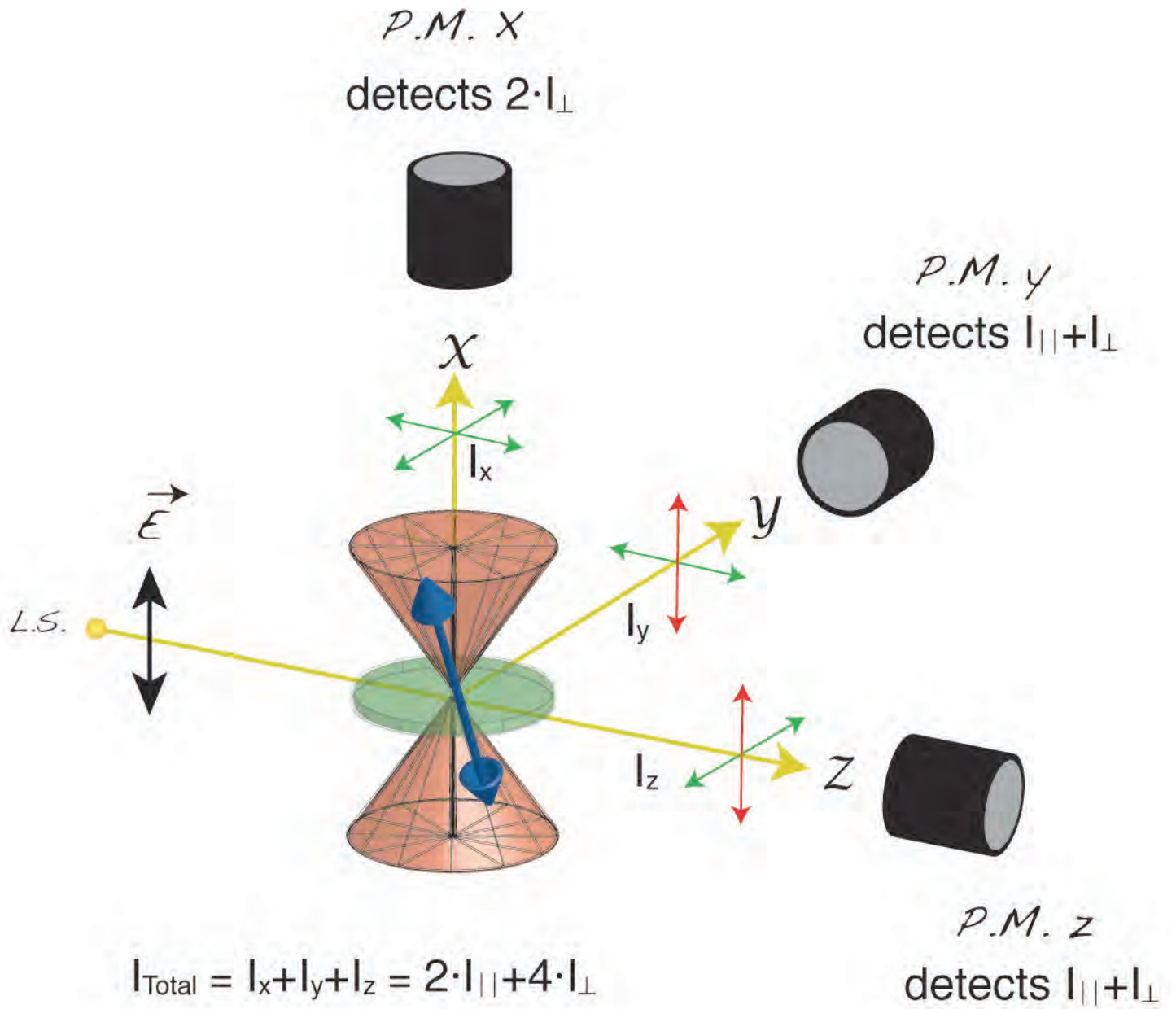


Figure 6

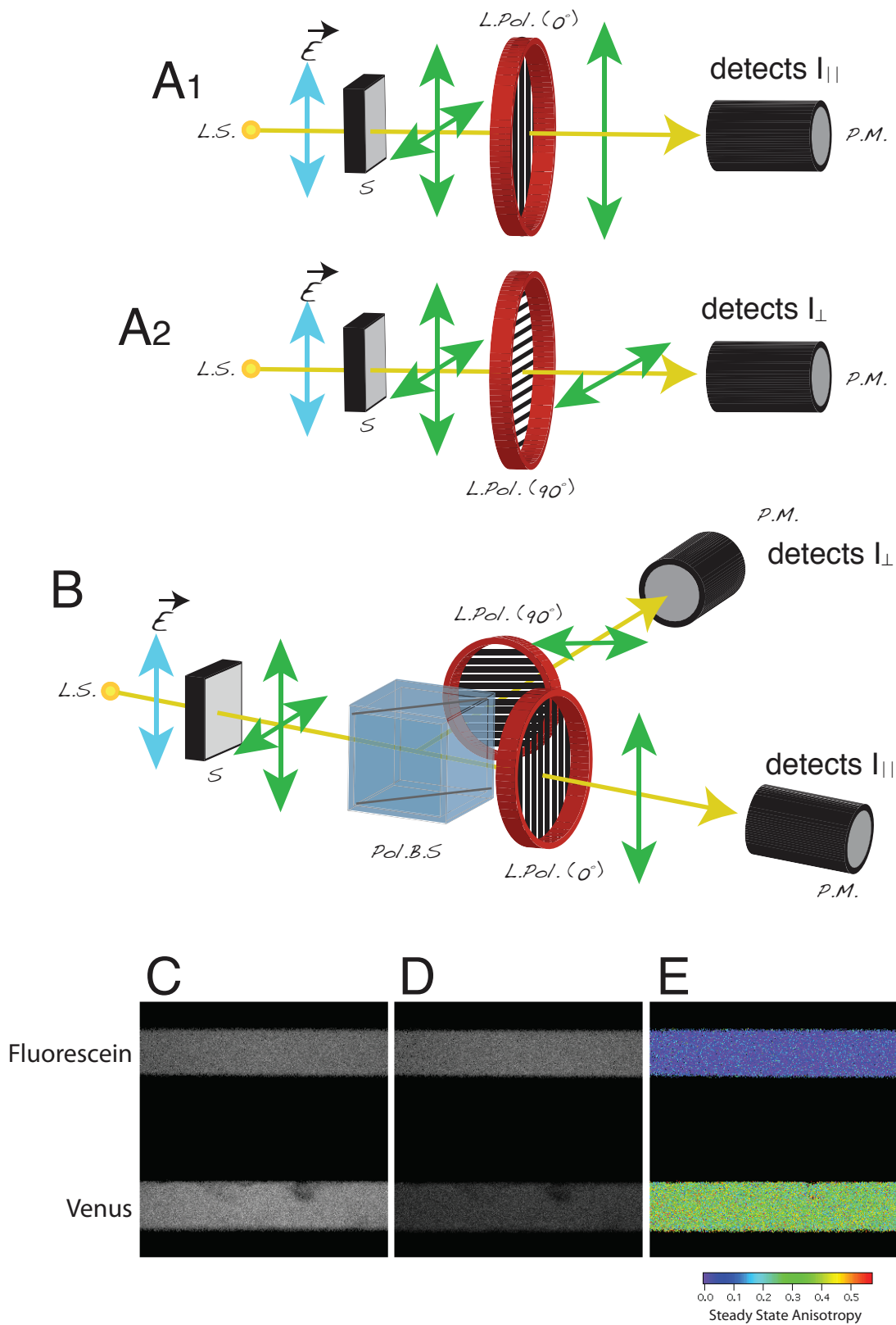


Figure 7

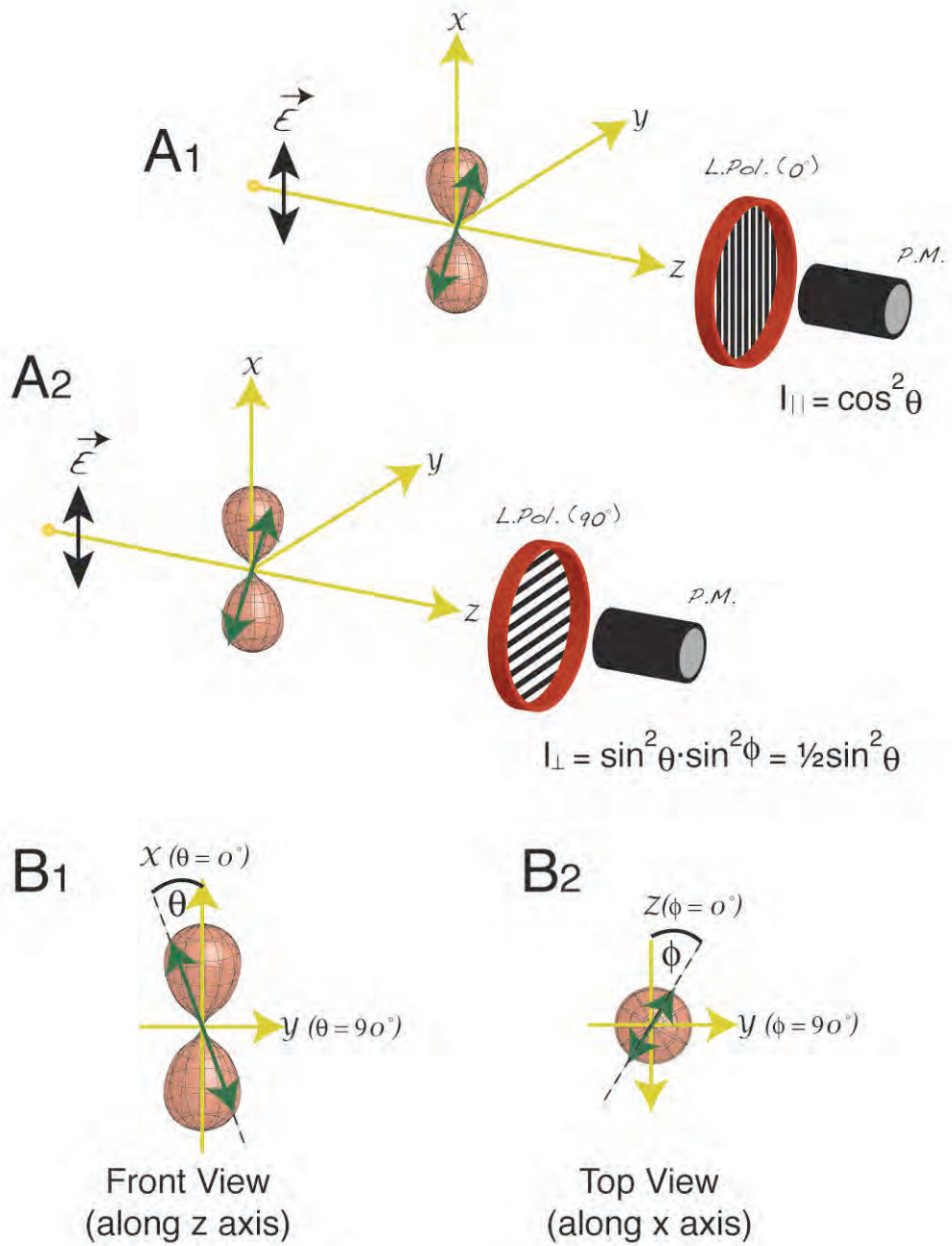


Figure 8

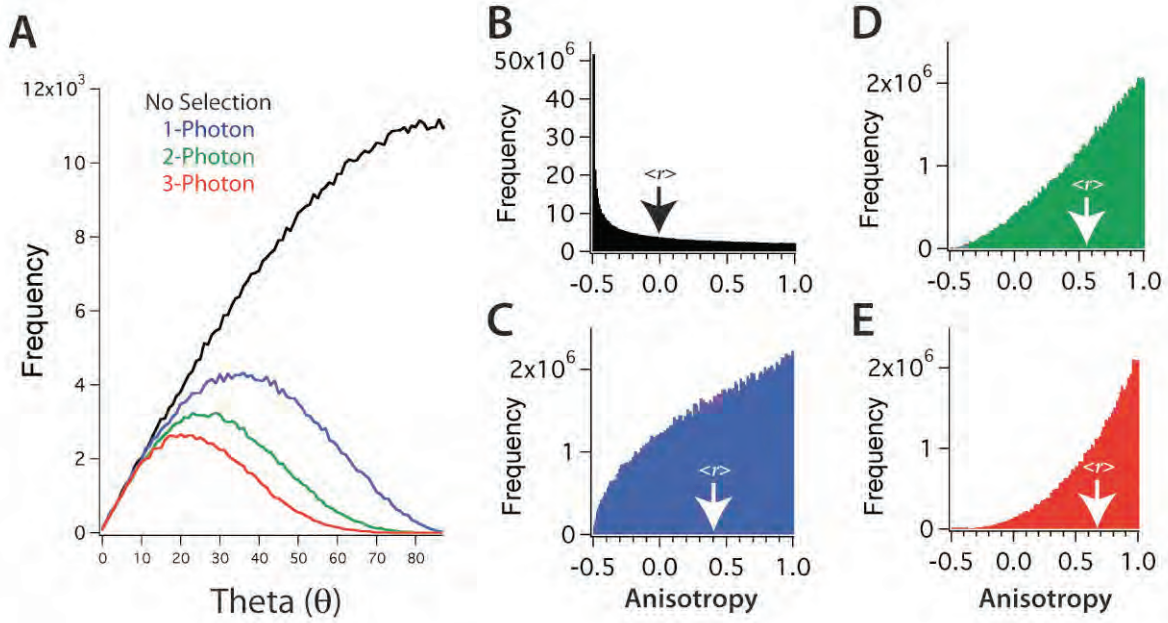


Figure 9

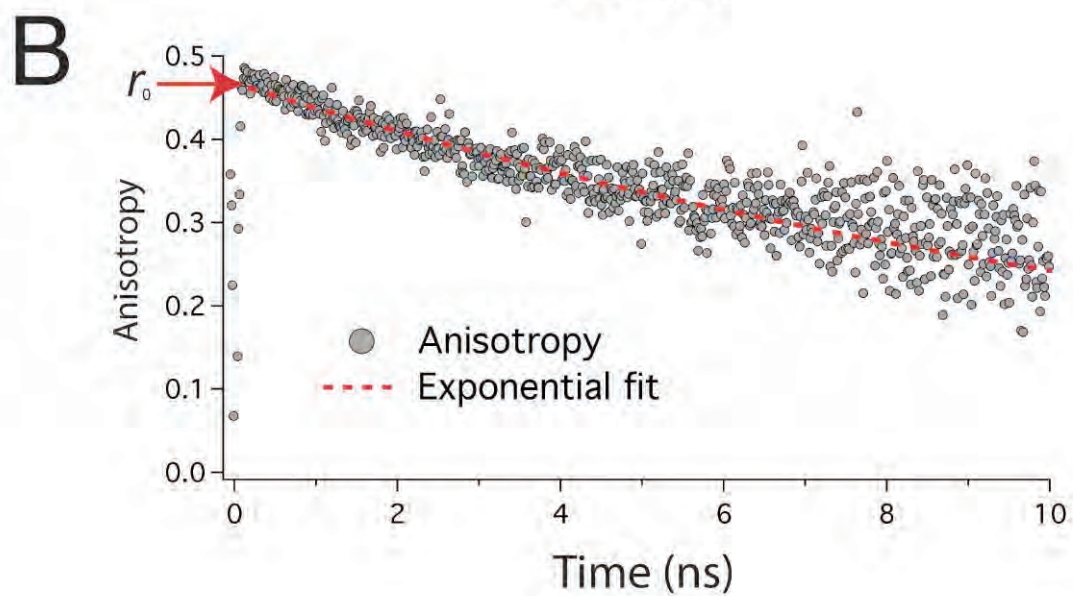
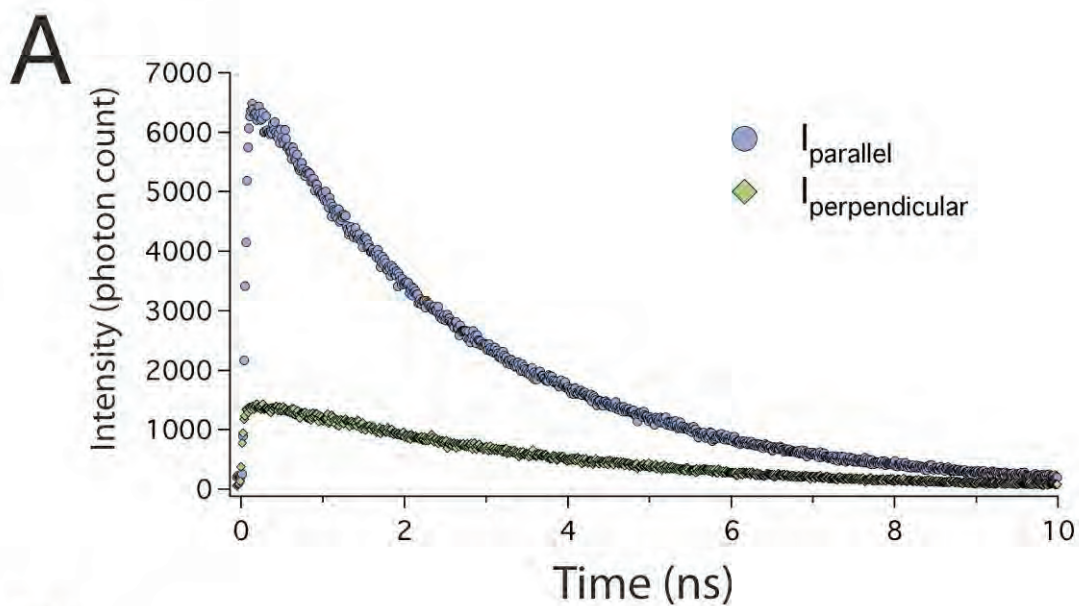


Figure 10

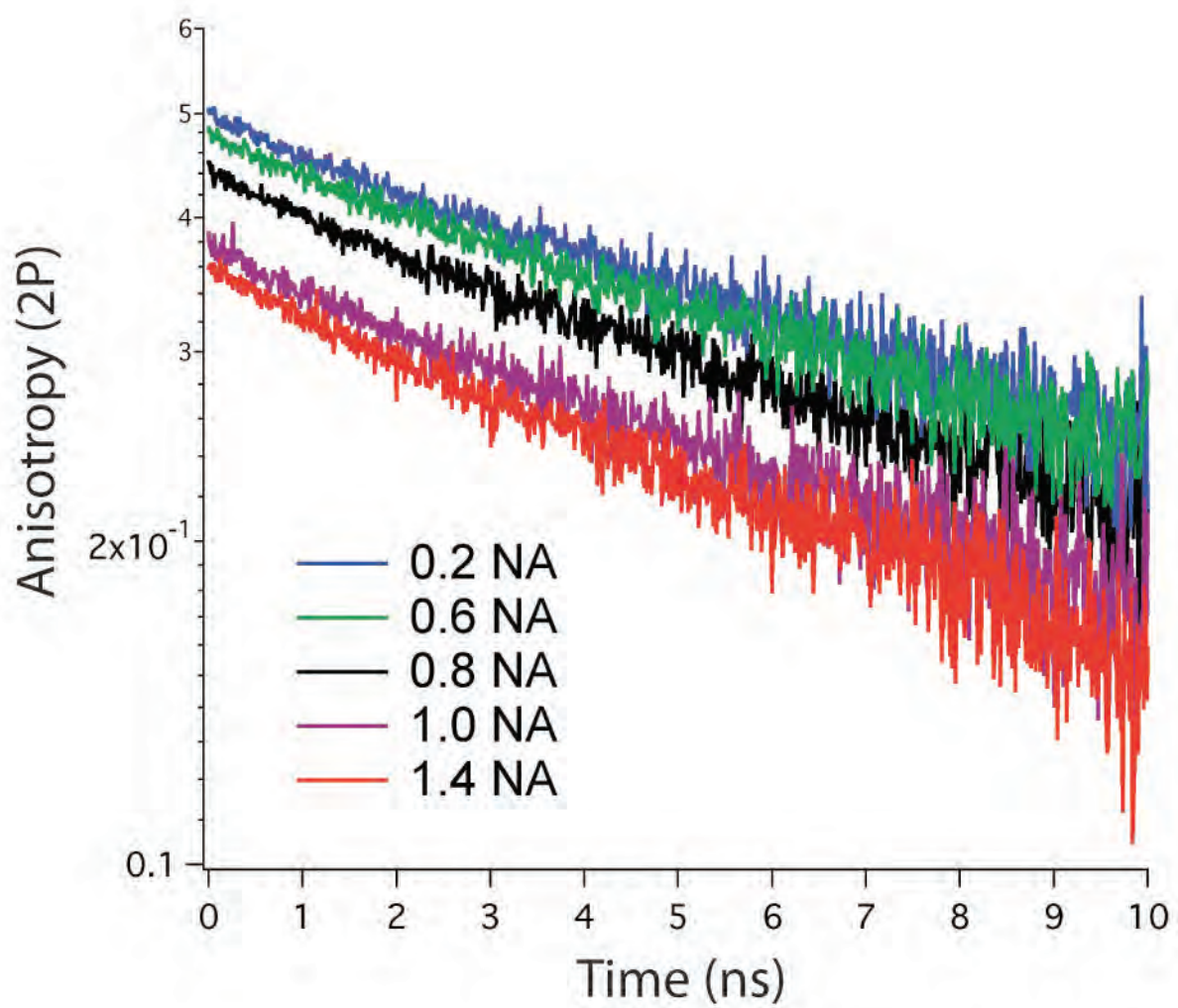


Figure 11

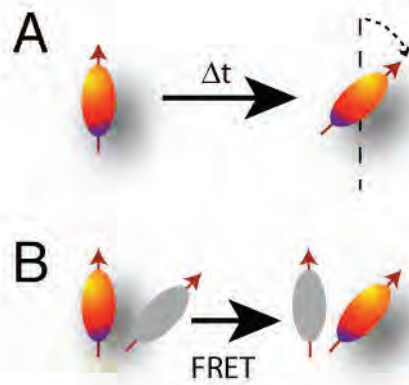


Figure 12

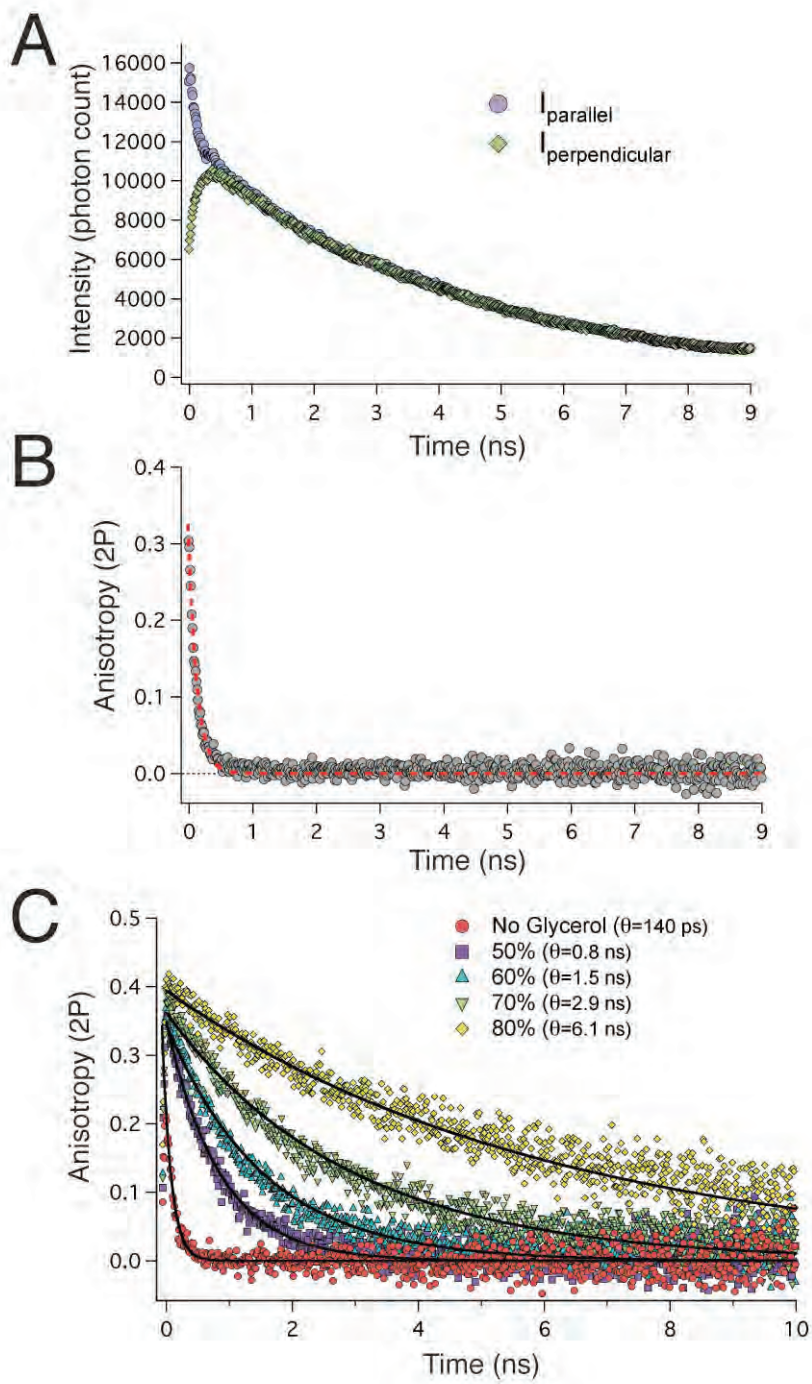


Figure 13

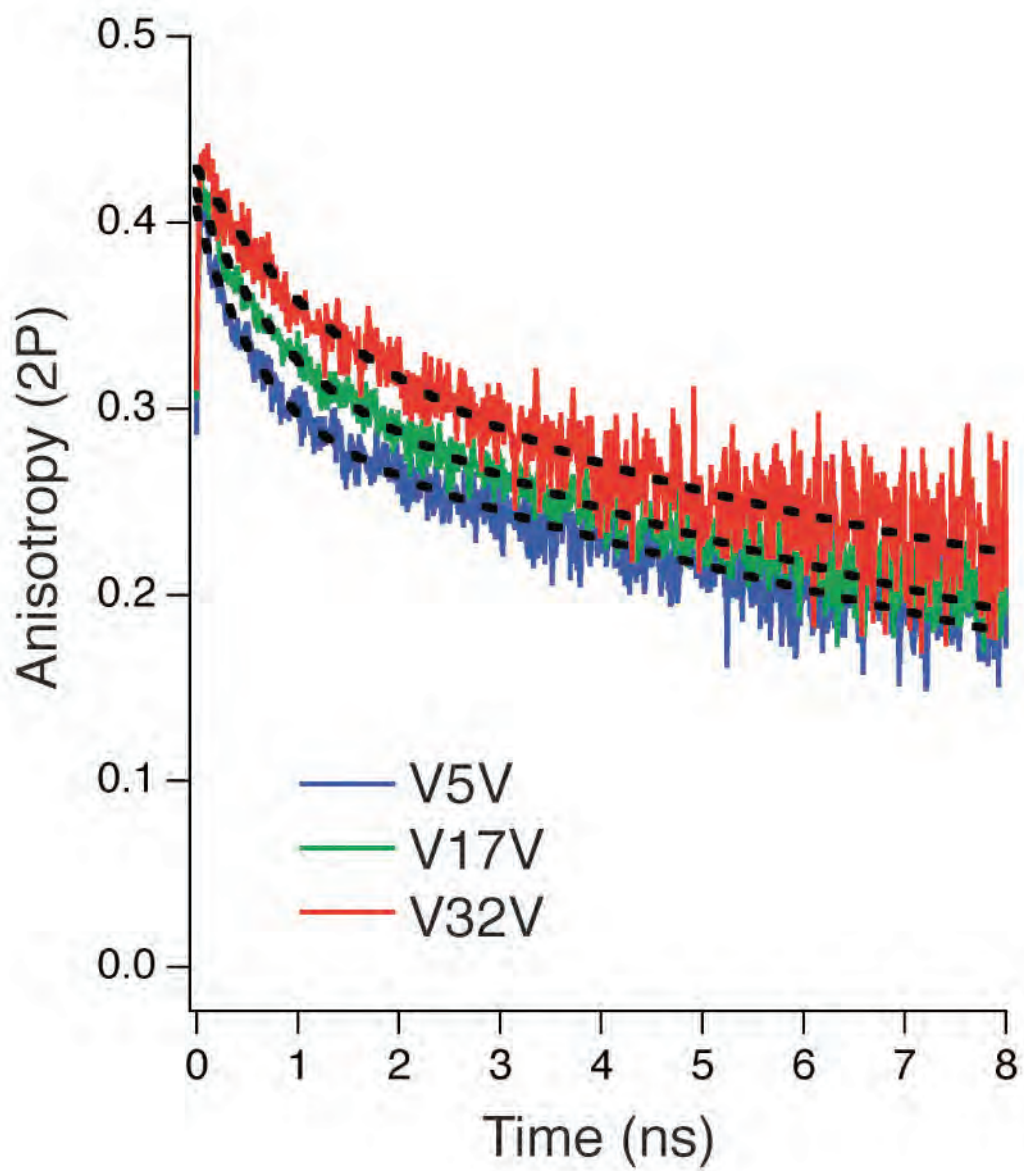


Figure 14

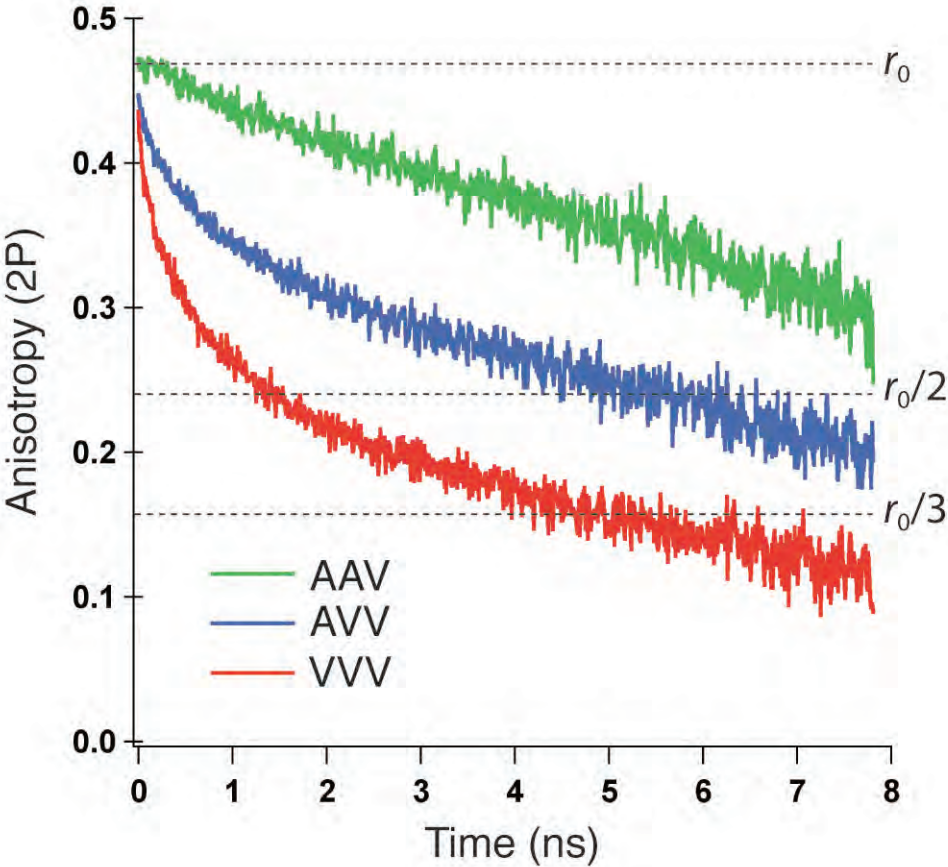


Figure 15

